# CHAPTER TWO ELECTRICAL RELAXATION [NO FIGURE VERSION]

# 1 2 3 4

# 4 **3/4/2017 4:09 AM**

# 5 Contents

6	PRELIMINARIES				
7	2.1	NOMENCLATURE	3		
8	2.2	ELECTROMAGNETISM	3		
9 10 11 12	2.2.1 2.2.2 2.2.3 2.2.3.1	UNITS ELECTROMAGNETIC QUANTITIES ELECTROSTATICS Point Charge (Coulomb's Law)	5 7		
12 13 14	2.2.3.1 2.2.3.2 2.2.3.3	Long Thin Rod with Uniform Linear Charge Density $\lambda$ Large Flat Insulating Plate	7		
15 16 17	2.2.3.4 2.2.3.5 2.2.3.6	Large Flat Conducting Plate Two Large Parallel Insulating Flat Plates Two Large Parallel Conducting Flat Plates	8		
18 19	2.2.3.7 2.2.3.8	Concentric Conducting Cylinders Concentric Conducting Spheres	9 9		
20 21 22	2.2.3.9 2.2.4 2.2.5	Isolated Sphere Electrodynamics Maxwell's Equations	10		
23 24 25	2.2.6 2.2.7 2.2.8	Electromagnetic Waves Local Electric Fields Circuits	16		
26 27	2.2.8 2.2.8.1 2.2.8.2	Simple Circuits AC Circuits	17 19		
28 29	2.2.8.3 2.3	Experimental Factors DIELECTRIC RELAXATION			
30	2.3.1	Frequency Domain	25		
31 32 33	2.3.1.1 2.3.1.2 2.3.2	Dipole Rotation Ionic Hopping TIME DOMAIN	30		
34 35	2.3.3 2.3.4	TEMPERATURE DOMAIN	31 33		
36 37 38	2.3.5 2.3.6 2.3.7	INTERFACIAL POLARIZATION Maxwell-Wagner Polarization Examples	35		
39 40 41	2.3.7.1 2.3.7.2 2.3.7.3	Liquid Water Supercooled Water Hydration Water	38		
42	2.4	CONDUCTIVITY RELAXATION	43		
43	2.4.1	GENERAL ASPECTS	43		

# Page 2 of 61

44	2.4.2	DISTRIBUTION OF CONDUCTIVITY RELAXATION TIMES	45		
45	2.4.3	Constant Phase Element Analysis			
46	2.4.4	Determination of $\sigma_{0}$			
47	2.4.4.1	Analyses in the Complex Resistivity Plane	48		
48	2.4.4.2	Modulus and Resistivity Spectra	48		
49	2.4.4.3	Complex Admittance Plane	49		
50	2.4.5	COMBINED CONDUCTIVITY AND DIELECTRIC RELAXATION			
51	2.4.6	Examples	50		
52	2.4.6.1	Electrode Polarization and Bulk Relaxation in the Frequency Domain	50		
53	2.4.6.2	Conductivity Relaxation in Sodium $eta$ – Alumina	51		
54	2.4.6.3	Complex Impedance Plane Analysis of Electrode Polarization in Sintered $eta-$ Alumina	52		
55	2.4.6.5	Intergranular Effects in Polycrystalline Electrolytes	53		
56	2.4.6.6	Intergranular Cracking	53		
57	2.4.6.7	Intergranular Gas Adsorption	54		
58	APPEN	DIX 2.1 – DERIVATION OF <i>M</i> * FOR A DEBYE RELAXATION WITH NO			
59		IONAL SEPARATE CONDUCTIVITY	56		
60	COMPI	JTATION CODE FOR A DEBYE RELAXATION WITH ADDITIONAL SEPA	RATE		
61		JCTIVITY $\sigma_0$			
01	CONDU				
62	APPEN	DIX 2.3 DERIVATION OF DEBYE DIELECTRIC EXPRESSION FROM			
63	EQUIVALENT CIRCUIT				
	-2010				
64					

66 Preliminaries (include in Book Prologue)

67 The examples used to illustrate different applications are not central to the purpose of this book and are not recent. Some of the applications have been discussed in an unpublished but 68 69 circulated paper by the present author that is available widely at 70 http://imhodge.startlogic.com/pdfs/ac%20data%20analysis(final).pdf.

71

# 72 2.1 Nomenclature

T3 Italicized lower case letters are used for physical variables, e.g.  $\{x, y, z, r\}$  for distances, *t* for time, and *q* for charge; italicized upper case letters are used for specific values of variables and field magnitudes, e.g.  $\{X, Y, Z, R\}$ , *T*, *Q*. Vectors are denoted by bold face upper case letters with an arrow  $\vec{V}$  and tensors are denoted by bold face upper case **T**.

There are two time constants for relaxation of polarization, one for relaxation at constant electric field (i.e. dielectric relaxation of the displacement  $\vec{D}$ ) denoted by  $\tau_E$  and one for relaxation at constant displacement (i.e. conductivity relaxation of the electric field  $\vec{E}$ ) denoted by  $\tau_D$ . Amongst other things these two distinct time constants correspond to two microscopic time constants for a single macroscopic dielectric time constant, as has been briefly discussed in ref. [1].

83 Dielectric and conductivity relaxations can both occur in the same material over two 84 resolvable frequency ranges and the usual nomenclature for the low and high frequency limits of 85 a single relaxation process (e.g.  $\varepsilon_0$  and  $\varepsilon_{\infty}$  for the relative permittivity) is ambiguous and has caused confusion in a long-standing debate about the legitimacy of the electric modulus 86 87 formalism. We introduce a new nomenclature here to distinguish the low and high frequency 88 limits for the two possible relaxations that, although somewhat clumsy, eliminates this confusion. The two limits for a dielectric relaxation at constant  $\vec{\mathbf{E}}$  are denoted by  $\varepsilon_0^E$  and  $\varepsilon_{\infty}^E$  and 89 the two limits for a conductivity relaxation at constant  $\vec{\mathbf{D}}$  are denoted by  $\varepsilon_0^D$  and  $\varepsilon_{\infty}^D$ . Since a 90 conductivity relaxation must occur at lower frequencies than a dielectric relaxation for the latter 91 92 to be readily observed (with some exceptions depending on instrumental sensitivity) then  $\mathcal{E}_{\infty}^{D} = \mathcal{E}_{0}^{E}$ . 93

94

Electric charge is denoted by q (Coulomb C), volume charge density by  $\rho$  (Cm<sup>-3</sup>),

95 surface charge density by  $\sigma \ C \ m^{-2}$ , linear charge density by  $\lambda \ C \ m^{-1}$ , current by *I* (Ampere = A =

96 C s<sup>-1</sup>), current density by  $J(Am^{-2})$ , electric potential by  $\varphi_E(V=JC^{-1})$ , electric field by E

- 97  $(NC^{-1} = Vm^{-1})$ , electric dipole moment by  $\mu_E$  (C.m), resistance by R (Ohm =  $\Omega = VA^{-1}$ ), and
- 98 capacitance by C (Farad  $F = CV^{-1}$ ). The SI unit for conductance (=1/resistance) is the Siemen S 99 (equal to  $\Omega^{-1}$ ).
- 100
- 101 2.2 Electromagnetism
- 102 2.2.1 Units

103 Two systems of electromagnetic units are in use, the cgs (centimeter-gram-second) and 104 the MKS (meter-kilogram-second) or SI (Systeme Internationale). The SI system is the official

### Page 4 of 61

105 scientific system but the cgs system appears in older publications and since it is still used by 106 chemists and materials scientists its relationship to the SI system is delineated here. For 107 mechanics only the numerical value of physical quantities changes with the system of units, but 108 in electromagnetism there is an additional difference of approach: electric charge in the cgs 109 system is defined in units of mass-length-time whereas in the SI it is defined to be just as 110 fundamental as mass, length and time: this SI unit of charge is the Coulomb. Other similar 111 non-electromagnetic differences occur: for example the SI temperature unit K (Kelvin) is also 112 considered to be a fundamental unit.

113 The cgs form of Coulomb's law for the force *F* between two point charges  $q_1$  and  $q_2$ 114 separated by a distance *r* and immersed in a medium of permittivity  $\varepsilon$  is

116 
$$F = \frac{q_1 q_2}{\varepsilon r^2} , \qquad (2.1)$$

117

121

115

118 that gives dimensions of  $M^{1/2}L^{3/2}T^{-1}$  for the *electrostatic unit* (esu) of charge. The cgs equation 119 for the magnetic force between two straight parallel conductors of length *L* carrying currents  $I_1$ 120 and  $I_2$  and separated by a distance *r* in a material of magnetic permeability  $\mu$  is

122 
$$F = \frac{2\mu L I_1 I_2}{r},$$
 (2.2)  
123

124 that gives dimensions of  $M^{1/2}L^{1/2}$  for the *electromagnetic unit* (emu) of charge. The esu and emu 125 units differ by a factor  $LT^{-1}$  that has the dimensions of speed and the value of the speed of light, 126 c. This is the reason that c enters into many cgs formulae. Numerically, emu = c esu (c in cgs 127 units =  $2.9979 \times 10^{10}$  cm/s).

128 The Coulomb C is defined experimentally by its time derivative, the current in *amperes* 129 A, that in turn is determined using eq. (2.2). A constant  $\mu_0$  is inserted into the SI form for this 130 magnetic force to ensure that the same force is produced by the same currents separated by the 131 same distance: 132

133 
$$F = \frac{\mu \mu_0 L I_1 I_2}{4\pi r}.$$
 (2.3)

134

Equations (2.2) and (2.3) reveal that  $\mu_0 = 4\pi \times 10^{-7}$  N.A<sup>-2</sup>. The factor  $4\pi$  arises from *Gauss's* Law (eq. (1.150) and eq. (2.18) below). The SI form of Coulomb's law is

138 
$$F = \frac{q_1 q_2}{4\pi \,\mathrm{e}_0 \varepsilon \,r^2},$$
 (2.4)

139

140 where  $e_0$  is a constant (the *permittivity* of free space) with dimensions  $Q^2 M^{-1} L^{-3} T^2$  that 141 correspond to the units of capacitance per unit length (Farads meter<sup>-1</sup>). Its numerical value is 142 8.854187818 ×10<sup>-12</sup> Farad m<sup>-1</sup>. The numerical relations between C, esu and emu are 143  $C \approx 3 \times 10^9 \text{ esu} \approx 10^{-1} \text{ emu}$ , where the approximate equality arises from placing the speed of 144 light at  $3 \times 10^8$  m/s rather than 2.9979...×10<sup>8</sup> m/s. The dimensionless fine structure constant  $\alpha$ 145 in cgs units is  $\alpha = e^2 / \hbar c = 2\pi e^2 / h c$  and in SI units is  $\alpha = 2\pi e^2 / 4\pi e_0 h c = e^2 / 2e_0 h c$ . It is 146 readily confirmed that this SI value of  $\alpha$  is dimensionless and has the same numerical value as 147 the cgs value. The quantity  $(e_0 \mu_0)^{-1/2}$  equals the speed of light so that  $e_0$  is 148  $e_0 = 1/c^2 \mu_0 = 1/(2.9979...\times 10^8)^2 (4\pi \times 10^{-7})$ .

149 The cgs system having been illustrated to this point is now dispensed with and only the SI 150 system is used from here on apart from some tabulated expressions and one occasional exception - the unit for the molecular dipole moment. In the SI system this is the coulomb-meter but this 151 152 unit is inconveniently large and is rarely used. The more common unit is the Debye, defined as the dipole moment created by two opposite charges of  $10^{-10}$  esu  $(3.3 \times 10^{-20} \text{ C})$  separated by 1.0 153 Angstrom  $(10^{-10} \text{ m})$ . The persistence of this unit probably originates in the facts that (a) 154 molecular dipole moments are of order unity when expressed in Debyes but of order  $10^{-30}$  in 155 coulomb-meters; (b) chemists and materials scientists still insist on using the Debye. It is not 156 clear to this author why a convenient SI unit such as  $10^{-31}$  C.m  $\approx 0.33$  Debye or  $10^{-30}$  C.m 157 158  $\approx 3.3$  Debye has not been introduced, especially since the SI unit nm has rapidly replaced the 159 Angstrom in optical spectroscopy.

# 160

#### 161 2.2.2 Electromagnetic Quantities

162 Many of these are conveniently defined using a parallel plate capacitor comprising two 163 conducting flat plates, each of area A and separated by a distance d. The geometric "cell 164 constant" k is

165  $k \equiv d / A$ .

(2.5)

Each plate has a charge of magnitude  $q_0$  but of opposite sign (uniformly distributed since the plates are conducting) that produces a potential difference V between the plates. The capacitance is  $C \equiv q_0 / V$  with unit Farad = C V<sup>-1</sup>. The surface charge density  $\sigma_0 = \pm q_0 / A$  on the plates induces an interfacial charge density  $\mp \sigma_i$  on each surface of any dielectric material between the plates. The *electric field*  $\vec{\mathbf{E}}$ , *polarization*  $\vec{\mathbf{P}}$  and *displacement vector*  $\vec{\mathbf{D}}$  are orthogonal to the plates with magnitudes defined by the following table:

172 173

174 175

$$\frac{SI}{D = \sigma_0} \frac{cgs}{D = 4\pi \sigma_0}$$
(2.6)

$$P = \sigma_i \qquad \qquad P = \sigma_i \tag{2.7}$$

176 
$$e_0 E = \sigma_0 - \sigma_i = D - P$$
  $E = 4\pi (\sigma_0 - \sigma_i) = D - 4\pi P$  (2.8)

177

178 The charge densities  $\sigma_0$  and  $\sigma_i$  generate an electrostatic potential  $\varphi_E$  (in volts) and net volume 179 charge density  $\rho$  for which

Page 6 of 61

181  $\vec{\mathbf{D}} = \nabla \rho$ 

182 and

183 
$$\vec{\mathbf{E}} = \nabla \varphi_E$$
. (2.10)

(2.9)

184

185 The inverse of eq. (2.10) is

186

187 
$$\varphi_{1,2} = \int_{s_1}^{s_2} \vec{\mathbf{E}} \cdot d\vec{\mathbf{s}}$$
(2.11)

188

189 where  $\vec{s}$  is the displacement vector in the direction of  $\vec{E}$  and  $\varphi_{1,2}$  is the potential difference 190 between the points  $s_1$  and  $s_2$ . The *relative permittivity*  $\varepsilon$  and *dielectric susceptibility*  $\chi_d$  are 191 defined in the following table:

192

193 
$$SI = cgs$$
  
194  $\varepsilon \equiv \frac{D}{e_0 E}$   $\varepsilon \equiv \frac{D}{E}$  (2.12)

195 
$$\chi_d = \frac{P}{e_0 E} = \frac{D - e_0 E}{e_0 E} = \varepsilon - 1$$
  $\chi_d = \frac{P}{E} = \frac{D - E}{4\pi E} = \frac{1}{4\pi} (\varepsilon - 1)$  (2.13)

A dielectric material between the plates decreases the electric field between the plates because the induced polarization charge density  $\sigma_i$  on the surface of the material partly cancels the unchanged charge density on the plates [eq. (2.8)]. The units of D and P (charge area<sup>-1</sup>) correspond to dipole moment (charge-distance) per unit volume. In view of  $\vec{D}$ ,  $\vec{E}$  and  $\vec{P}$  being vectors the relative permittivity and dielectric susceptibility are in general tensors but for isotropic media (liquids, glasses, and isotropic crystals) D, E, P and  $\varepsilon$  are all scalars. We mostly treat them as scalars in this book.

The magnetic analogs of *D*, *E*, *P*,  $e_0$ ,  $\varepsilon$  and  $\chi_d$  are, respectively, the magnetic induction *B*, the magnetic field *H*, the magnetization *M*, the permeability of free space,  $\mu_0$ , the relative permeability  $\mu$ , and the magnetic susceptibility  $\chi_m$ . The SI and cgs definitions are

$$\begin{array}{ccc}
207 & \underline{SI} & \underline{cgs} \\
208 & B = \mu_0 H & B = H
\end{array}$$
(2.14)

209 
$$M = \frac{B}{\mu_0} - H$$
  $M = \frac{B - H}{4\pi}$  (2.15)

210 
$$\mu = \frac{B}{H} \qquad \qquad \mu = \frac{B}{H} \qquad (2.16)$$

211 
$$\chi_M = \frac{M}{H} = \frac{B}{\mu_0 H} - 1$$
  $\chi_M = \frac{M}{H} = \frac{B}{4\pi H} - 1$  (2.17)

Page 7 of 61

212213 2.2.3 Electrostatics

214 Gauss's Law is

216 
$$\oint_{S} \mathbf{e}_{0} \varepsilon \vec{\mathbf{E}} \cdot d\vec{\mathbf{A}} = q_{enclosed} \Longrightarrow \oint_{S} \vec{\mathbf{D}} \cdot d\vec{\mathbf{A}} = q_{free}$$
(2.18)

217

215

where  $q_{\text{enclosed}}$  is the total net charge within a closed surface of magnitude A,  $\varepsilon$  is the relative 218 permittivity<sup>1</sup> of the material enclosed by the surface, and the surface integral is the flux of the 219 electric field through the surface. For the definition in terms of  $\vec{D}$  the quantity  $q_{tree}$  does not 220 include the induced polarization charges because these are subsumed into the permittivity  $e_0 \varepsilon$ . 221 Equation (2.18) is the electrical version of the mathematical Gauss's Theorem in Chapter One 222 [eq. 1.146)]. As noted in Chapter One the differential area vector  $d\vec{A}$  of a surface is defined as 223 224 having a direction perpendicular to the plane of the surface, and for closed surfaces such as occur 225 in Gauss's Law the outward pointing direction is defined to be positive. The Gaussian surface is 226 a purely mathematical object that can be placed anywhere although it must have the same symmetry as the system under study to be helpful. Thus information about charge distribution 227 228 can be inferred even though *E* is determined by the *total* enclosed charge.

229 We now apply Gauss's Law to calculate  $\vec{E}$  and the capacitance *C* for several electrical 230 geometries and charge distributions. The geometrical objects and charges are taken to be 231 immersed in a medium of relative permittivity  $\varepsilon$ .

## 233 2.2.3.1 Point Charge (Coulomb's Law)

234 Define the Gaussian surface *S* as a sphere of radius *r* with a point charge *q* at its center. 235 By symmetry  $\vec{\mathbf{E}}$  is everywhere parallel to  $d\vec{\mathbf{a}}$  and has a constant magnitude *E* obtained from 236  $e_0 \varepsilon \oint \vec{\mathbf{E}} \cdot d\vec{\mathbf{A}} = 4\pi r^2 e_0 \varepsilon E$  so that

237

232

238 
$$E = \frac{q}{4\pi\varepsilon e_0 r^2}$$
. (2.19)

239

240 2.2.3.2 Long Thin Rod with Uniform Linear Charge Density  $\lambda$ 

Let the Gaussian surface be a cylinder of radius r and length L, with the rod as its coaxial central axis. Then  $\varepsilon e_0 \oint_{S} \vec{E} \cdot d\vec{A} = \varepsilon e_0 E(2\pi rL) = q = \lambda L$  so that at a distance r from the

- 243 axis
- 244

<sup>&</sup>lt;sup>1</sup> Too often called the "dielectric constant" which is misleading because it is not constant (it varies with temperature and frequency for example).

245 
$$E = \frac{\lambda}{2\pi\varepsilon e_0 r}.$$
 (2.20)

246

247 2.2.3.3 Large Flat Insulating Plate

Let a charge q be uniformly distributed over the two sides of an infinite<sup>2</sup>, flat insulating plate of area A so that the charge on each surface is q/2. Define  $\sigma$  as the charge per unit area so that the charge density on each surface is  $\sigma/2$ . Define the Gaussian surface as a cylinder whose axis is parallel with the area vector of one plate and has one end inside the plate and the other end in a medium of relative permittivity  $\varepsilon$ . Then the electric field points away from each surface of the plate (since q is positive) and  $\varepsilon e_0 \oint \vec{E} \cdot d\vec{A} = \varepsilon e_0 E(A) = q/2 = \sigma A/2$  so that

254

258

$$E = \frac{\sigma}{2e_0 \varepsilon}.$$
(2.21)

257 The electric field is therefore independent of distance from the plate.

259 2.2.3.4 Large Flat Conducting Plate

Let the charge on each side of the plate be q/2 and define the Gaussian surface to be the 260 same as that for the insulating plate in §2.2.3.3. The electrostatic field inside a conductor is zero 261 262 that the electric field points away each surface of the plate SO and . → . . hat

263 
$$e_0 \varepsilon \bigoplus_{s} \mathbf{E} \cdot \mathbf{dA} = e_0 \varepsilon E(A) = q/2 = \sigma A/2$$
 so the

264

$$E = \frac{\sigma}{2\varepsilon e_0} \,. \tag{2.22}$$

266

268

267 This electric field again does not depend on distance from the plate.

## 269 2.2.3.5 Two Large Parallel Insulating Flat Plates

270 Consider charges  $\pm q$  that are uniformly distributed over the two surfaces of each plate. 271 The field between the plates is the vector sum of the fields from each plate. Since the field from 272 the positively charged plate points away from the positive plate and the field from the negatively 273 charged plate points toward the negative plate the two fields add up as vectors to 274

275 
$$E = \frac{\sigma}{\varepsilon e_0}.$$
 (2.23)

276

278

277 2.2.3.6 Two Large Parallel Conducting Flat Plates

The charges  $\pm q$  on each plate are attracted to the opposite charges on the other plate so

<sup>&</sup>lt;sup>2</sup> "Infinite" in extent relative to the distance between the plate in order to eliminate edge effects.

that the charges on each plate will lie totally on the inside surface and the charge density on each interior surface is  $\sigma = q/A$ . Since the effect of one plate on the other has been taken into account in this case the electric fields do *not* add up and the field between the plates is again 282

$$E = \frac{\sigma}{\varepsilon e_0}.$$
(2.24)

284

The charge density on the outer surface of each plate is zero so that the electric field outside the plates is also zero. Since eq. (2.6) equates  $\sigma$  to *D* eq. (2.23) yields  $E = D/e_0 \varepsilon$ , i.e. eq. (2.12).

287 The capacitance is obtained from the voltage difference V = E.d V between the plates 288 and  $q = A\sigma_0$ :

289

290 
$$C = \frac{q}{V} = \frac{\sigma_0 A}{Ed} = \frac{\sigma_0 A/d}{e_0 \varepsilon / \sigma_0} = (A/d)(e_0 \varepsilon) = (e_0 \varepsilon / k).$$
(2.25)

291

292 2.2.3.7 Concentric Conducting Cylinders

Let the inner and outer radii of two concentric conducting cylindrical plates be *a* and *b*, respectively, let their equal height be *h*, and let charges +q and -q be uniformly distributed on the inside surfaces of each plate. Form a concentric cylindrical Gaussian surface of radius a < r < b and height *h*, so that  $\oint_{s} \vec{\mathbf{E}} \cdot d\vec{\mathbf{A}} = E(2\pi rh) = q/e_0\varepsilon$ . Then  $E = q/(2\pi rhe_0\varepsilon)$  so that

297

298 
$$V = \int_{a}^{b} E dr = \left(\frac{q}{2\pi\hbar e_{0}\varepsilon}\right)_{a}^{b} \frac{dr}{r} = \frac{q}{2\pi\hbar e_{0}\varepsilon}\ln\left(\frac{b}{a}\right)$$
(2.26)

299

301

300 and the capacitance is

$$302 \qquad C = \frac{q}{V} = \frac{2\pi h e_0 \varepsilon}{\ln\left(\frac{b}{a}\right)} \tag{2.27}$$

303

304 2.2.3.8 Concentric Conducting Spheres

305 Let the inner and outer radii of two concentric spherical conducting plates be *a* and *b*, 306 respectively, and let charges +q and -q reside on the inside surfaces of each plate. Form a 307 concentric spherical Gaussian surface of radius a < r < b, so that  $\oint_{s} \vec{\mathbf{E}} \cdot d\vec{\mathbf{A}} = E[4\pi r^{2}] = q/e_{0}$ 308 and  $E = q/[4e_{0}\pi r^{2}]$ . Then

310 
$$V = \int_{a}^{b} E dr = \frac{q}{4\pi e_0 \varepsilon} \int_{a}^{b} \frac{dr}{r^2} = \frac{q}{4\pi e_0 \varepsilon} \left(\frac{1}{b} - \frac{1}{a}\right) = \frac{q}{4\pi e_0 \varepsilon} \left(\frac{a - b}{ab}\right)$$
(2.28)

311 312

312 and  
313 
$$C = \frac{q}{V} = 4\pi e_0 \varepsilon \left(\frac{ab}{b-a}\right).$$
(2.29)

314

315 2.2.3.9 Isolated Sphere

The capacitance of an isolated sphere is obtained from eq. (2.29) by taking the limit  $b \rightarrow \infty$  and for convenience placing a = R:

 $319 \qquad C = 4\pi e_0 \varepsilon R. \tag{2.30}$ 

320

322

318

321 Thus larger spheres have larger capacitances.

Electric current, symbol *I*, is defined as

323 2.2.4 Electrodynamics

Consider a constant voltage *V* applied across two parallel plates between which there is now a conducting medium. Let the resistivity of the material be  $\rho = R.k^{-1}$  (units ohm-meter) and specific conductivity  $\sigma = 1/\rho$  (units S m<sup>-1</sup>), where *R* is the resistance between the plates in ohms and the symbol S refers to the SI unit Siemen defined as the reciprocal of the ohm. The current density  $\vec{J}$  is the electric current per unit (orthogonal) area (units A m<sup>-2</sup>) so that  $\vec{J}\rho = \vec{E}$ . Unfortunately the displacement current  $dD/dt = d\sigma_0/dt$  (better named as the displacement current density) has no symbol.

331332

$$I = \frac{dq}{dt}$$

$$(2.31)$$

$$334$$

so that the total charge that passes across a plane through which a current I flows is

337 
$$q = \int_{0}^{t} I \, dt'$$
. (2.32)

338

336

339 The electric potential  $\varphi_E$  is not defined for electrodynamics (see §2.5 below on Maxwell's 340 equations) and is replaced by the symbol voltage V (unfortunately also used for the unit volt). 341 Ohm's Law for the electrical resistance R (SI unit ohm ( $\Omega$ ) is then

342

$$R \equiv \frac{V}{I} \tag{2.33}$$

344

and  $\Omega = V/A$ . An electrical conductor is said to be ohmic if, and only if, *R* is constant. This is not the same as dV/dI = constant: for example if V = 1.0 + 2I and dV/dI = 2 then  $R = 3\Omega$  for I = 1A,  $R = 2.5\Omega$  for I = 2A,  $R = 2.3\Omega$  for I = 3A. Resistances dissipate power *P* given by P = IV (recall that energy is given by QV and power is the time derivative of energy). For ohmic resistances

$$350$$

$$P = IV$$

351 
$$= I(IR) = I^2R$$
  
=  $(V/R)V = V^2/R$ . (2.34)

- 352
- 353 2.2.5 Maxwell's Equations

These four equations summarize all that is known about electromagnetic phenomena – they are essentially the electromagnetic equivalent of Newton's laws for mechanics but more mathematically sophisticated because of the greater complexity of electromagnetic phenomena. The differential forms of the four Maxwell equations are:

358  $359 \quad \vec{\nabla} \cdot \vec{\mathbf{D}} = \rho ; \tag{2.35}$ 

$$360 \quad \vec{\nabla} \cdot \vec{\mathbf{B}} = 0; \tag{2.36}$$

$$361 \qquad \vec{\nabla} \times \vec{\mathbf{E}} = -\left(\frac{\partial \vec{\mathbf{B}}}{\partial t}\right); \tag{2.37}$$

$$362 \qquad \vec{\nabla} \times \vec{\mathbf{H}} = \vec{\mathbf{J}} + \left(\frac{\partial \vec{\mathbf{D}}}{\partial t}\right) \tag{2.38}$$

$$363 \qquad = \sigma \vec{\mathbf{E}} + \left(\frac{\partial \vec{\mathbf{D}}}{\partial t}\right) \tag{2.39}$$

364 
$$= \sigma \vec{\mathbf{E}} + \mathbf{e}_0 \left( \frac{\partial \varepsilon \vec{\mathbf{E}}}{\partial t} \right).$$
(2.40)

365

367

366 For a vacuum equation (2.38) is equivalent to

368  $\vec{\nabla} \times \vec{\mathbf{B}} = \mu_0 \vec{\mathbf{J}} + \mu_0 \mathbf{e}_0 \left( \frac{\partial \vec{\mathbf{E}}}{\partial t} \right)$  (2.41)

where  $\sigma$  is the specific electrical conductivity (units  $(\Omega^{-1}m^{-1} = Sm^{-1})$ ,  $\vec{B}$  is the magnetic 369 370 induction, and  $\vec{\mathbf{H}}$  is the magnetic field. Equations (2.38) - (2.40) merit amplification. The 371 equation  $\vec{\nabla} \times \vec{\mathbf{H}} = \vec{\mathbf{J}}$  might perhaps be expected instead of eq. (2.38) but this has the nonsensical implication that there could never be any sources or sinks of current anywhere at any time, 372 because the vector identity  $\vec{\nabla} \cdot (\vec{\nabla} \times \vec{\mathbf{H}}) = 0$  would then imply  $\vec{\nabla} \cdot \vec{\mathbf{J}} = 0$ . The difficulty is resolved 373 374 by noting that for a charging or discharging parallel plate capacitor (for example) charge flow in the external circuit joining the two capacitor plates, corresponding to  $dq_0/dt$  where  $q_0$  is the 375 charge on the capacitor plates (see §2.1.2 above), must be compensated for by an opposite 376 377 change of the polarization charges between the plates (to ensure charge conservation). Thus 378

Page 12 of 61

379 
$$\vec{\nabla} \cdot \left(\vec{\nabla} \times \vec{\mathbf{H}}\right) \equiv 0 = \vec{\nabla} \left[ \left( \frac{\partial q_0}{\partial t} \right) - \left( \frac{\partial q_i}{\partial t} \right) \right]$$
 (2.42)

is ensured.

381 The term  $\partial \vec{\mathbf{D}} / \partial t$  in eq. (2.38) can correspond for example to a localized (molecular 382 diameter) effective spatial translation of charge due to rotation of an electric dipole about its center of mass that has a close analogy to an ion hopping to an adjacent site (see §2.2.1.2). It is 383 called the displacement current. The term displacement "current" has been claimed to be a 384 misnomer but this is true only if a current is interpreted to be a long range translational migration 385 of charge. If the definition of current as dq/dt is adopted it is not a misnomer because q (on 386 capacitor plates for example) changes with time [eq. (2.42)], and furthermore a traditional 387 current must be present in an external circuit to compensate for  $\partial q_i / \partial t$ . Describing  $\partial \vec{\mathbf{D}} / \partial t$  as a 388 389 "fictitious current", as has been done in at least one popular text book, is disingenuous and misleading because eq. (2.38) demonstrates that  $\partial \vec{\mathbf{D}} / \partial t$  is just as important in determining a 390 magnetic field as migration of individual charges. 391



### The vector potential $\vec{\mathbf{A}}$ is defined by

$$\vec{\nabla} \times \vec{\mathbf{A}} = \vec{\mathbf{B}} \tag{2.43}$$

395

396 and 397

$$398 \qquad \vec{\mathbf{E}} = -\vec{\nabla}\varphi_E - \frac{\partial\vec{\mathbf{A}}}{\partial t}, \qquad (2.44)$$

399

and is introduced essentially to ensure consistency between electrostatics and electrodynamics. Equation (2.43) ensures eq. (2.36) because of the vector identity  $\vec{\nabla} \cdot (\vec{\nabla} \times \vec{A}) = 0$  and eqs. (2.43) and (2.44) together ensure that eq. (2.37) remains true in dynamic situations where  $\varphi_E$  is undefined. The vector potential is essentially an extension of the Coulomb potential  $\varphi_E$  to dynamic situations because the definition of  $\varphi_E$  from  $\vec{E} = \nabla \varphi_E$  [eq. (2.10)] is definable only in static situations, as the following consideration indicates: if  $\partial \vec{B} / \partial t \neq 0$  then  $\vec{\nabla} \times \vec{E} \neq 0$  by eq. (2.36) and the static relation

$$408 \qquad \mathbf{\dot{E}} = \nabla \varphi_E \tag{2.45}$$

409

410 could then never hold because of the vector identity  $\vec{\nabla} \times (\vec{\nabla} \varphi_E) = 0$ . But  $\vec{\mathbf{E}}$  is known to be 411 nonzero in dynamic situations (Ohm's Law!). Similarly if  $\vec{\mathbf{J}} \neq 0$  or  $\partial \vec{\mathbf{D}} / \partial t \neq 0$  then there is 412 no potential  $\varphi_B$  for  $\vec{\mathbf{B}}$  (defined by  $\vec{\mathbf{B}} = \vec{\nabla} \varphi_B$ ) because eq. (2.38) then implies

(2.50)

413  $\vec{\nabla} \times \vec{\mathbf{H}} = \vec{\nabla} \times \vec{\mathbf{B}} / \mu \mu_0 \neq 0$  because of the same vector identity  $\vec{\nabla} \times (\vec{\nabla} \varphi_B) = 0$ . Both these 414 difficulties are averted by the introduction of  $\vec{\mathbf{A}}$ . Equation (2.44) is then consistent with eq. 415 (2.37) since it guarantees

416

417 
$$\vec{\nabla} \times \vec{\mathbf{E}} = \vec{\nabla} \times \left( -\vec{\nabla} \, \boldsymbol{\varphi}_E - \frac{\partial \vec{\mathbf{A}}}{\partial t} \right) = -\frac{\partial \vec{\mathbf{B}}}{\partial t}.$$
 (2.46)

418 419

Integral versions of Maxwell's equations include Faraday's Law:

420

421 
$$\oint \vec{\mathbf{E}} \cdot d\vec{\mathbf{s}} = -\frac{d\Phi_B}{dt}; \quad \Phi_B \equiv \oint \vec{\mathbf{B}} \cdot d\vec{\mathbf{A}} = \text{magnetic flux}$$
 (2.47)

422

424

423 and Ampere's law

- 425  $\oint \vec{\mathbf{B}} \cdot d\vec{\mathbf{s}} = \mu_0 \mathbf{e}_0 \frac{d\Phi_E}{dt} + \mu_0 I_{enclosed}; \quad \Phi_E \equiv \oint \vec{\mathbf{E}} \cdot d\vec{\mathbf{A}} = \text{electric flux}$ (2.48)
- 426

427 Equation (2.40) provides a convenient means for demonstrating the equivalence of the 428 complex permittivity and complex conductivity. First convert eq. (2.40) from a vector equation 429 to a complex scalar equation:

431 
$$\vec{\nabla} \times \vec{\mathbf{H}} = \sigma \vec{\mathbf{E}} + \mathbf{e}_0 \left( \frac{\partial \varepsilon \vec{\mathbf{E}}}{\partial t} \right) \Rightarrow \left| \vec{\nabla} \times \vec{\mathbf{H}} \right| = \sigma * E * + \mathbf{e}_0 \varepsilon * \left( \frac{\partial E *}{\partial t} \right).$$
 (2.49)

432

430

433 For a sinusoidal excitation  $E^* = E_0 \exp(-i\omega t)$  eq. (2.49) becomes

434

$$\begin{aligned} \left| \vec{\nabla} \times \vec{\mathbf{H}} \right| &= \sigma^* E_0 \exp(-i\omega t) - e_0 \varepsilon^* E_0 (i\omega) \exp(-i\omega t) \\ 435 &= \left[ \sigma^* - i\omega e_0 \varepsilon^* \right] E_0 \exp(-i\omega t) \\ &= \left[ \varepsilon^* - \sigma^* / (i\omega e_0) \right] (-ie_0 \omega) E_0 \exp(-i\omega t), \end{aligned}$$

436

437 indicating that both the complex conductivity  $[\sigma^* - i\omega e_0 \varepsilon^*]$  and complex permittivity 438  $[\varepsilon^* - \sigma^*/(i\omega e_0)]$  provide equivalent descriptions of electrical relaxation, as do the resistivity 439  $\rho^* = 1/\sigma^*$  and electric modulus  $M^* = 1/\varepsilon^*$ . All these different functions emphasize or 440 suppress different facets of experimental data in the same way that Fourier transforms do for 441 example [see eq. (2.106) below].

- 442
- 443 2.2.6 Electromagnetic Waves
- 444 The Maxwell equations together with the constitutive relations  $\mathbf{D} = \mathbf{e}_0 \varepsilon \mathbf{E}$  and  $\mathbf{B} = \mu_0 \mu \mathbf{H}$ 445 predict transverse electromagnetic (em) waves traveling at the speed of light c/n

446

447 
$$\frac{c}{n} = \frac{\left(1/e_0\mu_0\right)^{1/2}}{\left(\varepsilon\mu\right)^{1/2}} = \frac{1}{\left(e_0\varepsilon\mu_0\mu\right)^{1/2}},$$
(2.51)

448

449 where 450

451 
$$n = (\varepsilon \mu)^{1/2}$$
 (2.52)  
452

453 is the refractive index. In a nonmagnetic material for which  $\mu = 1$  and  $\varepsilon^* = (n^*)^2$ 

454  
455 
$$(n^*)^2 = (n'-in'')^2 = (n'^2 - n''^2) - 2in'n'' = \varepsilon^* = \varepsilon' - i\varepsilon''$$
  
456
  
(2.53)

457 so that

458  
459 
$$\varepsilon' = n'^2 - n''^2$$
  
460 and (2.54)

461

$$\begin{array}{ll}
462 & \varepsilon'' = 2n'n''. \\
463 & & (2.55)
\end{array}$$

464 For the general case of a magnetic material where the relative magnetic permeability is also 465 complex,  $\mu^* = \mu' - i\mu''$ ,

466

467 
$$(n^*)^2 = (n^{\prime 2} - n^{\prime 2}) - 2in'n'' = (\varepsilon' - i\varepsilon'')(\mu' - i\mu'')$$
 (2.56)

468

469 so that470

471 
$$(n^*)^2 = (n^{\prime 2} - n^{\prime 2}) - 2in^{\prime}n^{\prime \prime} = (\varepsilon^{\prime} - i\varepsilon^{\prime \prime})(\mu^{\prime} - i\mu^{\prime \prime}) = (\varepsilon^{\prime}\mu^{\prime} - \varepsilon^{\prime \prime}\mu^{\prime \prime}) - i(\varepsilon^{\prime}\mu^{\prime \prime} + \varepsilon^{\prime \prime}\mu^{\prime}),$$
 (2.57)

472

473 and 474

475 
$$n'' = \left(\varepsilon' \mu'' + \varepsilon'' \mu'\right). \tag{2.58}$$

476

Thus absorption of electromagnetic energy by magnetically lossy materials is enhanced by a highrelative permittivity.

479 The electric field component of a plane electromagnetic traveling wave of angular 480 frequency  $\omega$  propagating in the +x direction in a medium with refractive index n and speed c/n 481 is

482 
$$E(x,t) = E_0 \exp\left\{-i\omega\left[t - \frac{nx}{c}\right]\right\},$$
 (2.59)

and similarly for the magnetic field component. For complex  $n^* = n' - in''$  eq. (2.59) becomes 485

$$E(x,t) = E_0 \exp\left\{-i\omega \left[t - \frac{(n'-n'')x}{c}\right]\right\}$$

$$= E_0 \exp\left\{-i\omega \left[t - \frac{n'x}{c}\right]\right\} \exp\left[\frac{-n''\omega x}{c}\right]$$
(2.60)

487

483

488 so that *E* decays exponentially with distance +*x* into the medium. The intensity  $I = |E|^2$  of em 489 waves is then

490

$$I = E_0^2 \exp\left\{-2i\omega\left[t - \frac{(n' - in'')x}{c}\right]\right\}$$

$$= E_0 \exp\left\{-2i\omega\left[t - \frac{n'x}{c}\right]\right\} \exp\left[\frac{-2n''\omega x}{c}\right]$$
(2.61)

492

494

493 that is to be compared with Beer's Law

495 
$$I = I_0 \exp(-\alpha x),$$
 (2.62)

496

497 where  $\alpha$  is the extinction coefficient (usually expressed in neper m<sup>-1</sup> where the dimensionless 498 neper is used to emphasize that the logarithmic form of eq. (2.62) implies the Naperian 499 logarithm). Equations (2.61) and (2.62) yield

501 
$$\alpha(\omega) = \frac{2\omega n''(\omega)}{c}$$
. (2.63)

502

500

503 Observe the sign convention for imaginary numbers mentioned in the Introduction of 504 Chapter One at work here. If the sinusoidal perturbation was defined as  $E(x,t) = E_0 \exp\{+i\omega[t - nx/c]\}$  and the sign of the imaginary component of  $\varepsilon^*$  remained 505 negative then  $\alpha$  would have to be negative and Beer's Law would predict unphysical 506 507 exponential growth through a medium. This can be resolved by making the imaginary component of  $\varepsilon^*$  positive but this corresponds to a dipole rotation that leads the excitation 508 voltage rather than lags it. Nonetheless this is the convention used by electrical engineers and is 509 510 the price paid for the "advantage" of having a positive sign in the complex exponential. An 511 excellent account of phase conventions is given in Chapter One of ref. [2].

- 512 Insertion of eq. (2.55) into eq. (2.63) yields
- 513

Page 16 of 61

514 
$$\alpha(\omega) = \frac{\omega \varepsilon''(\omega)}{n'(\omega)c},$$
 (2.64)

515

516 and since  $\varepsilon'' = \sigma'/(e_0\omega)$  then

517

518 
$$\alpha(\omega) = \frac{\sigma'(\omega)}{n'(\omega)e_0c}.$$
 (2.65)

519 Thus  $n'', \varepsilon'', \alpha$  and  $\sigma'$  are all measures of absorption of electrical energy:

520 
$$\alpha = \frac{\sigma'}{ne_0c} = \frac{\omega\varepsilon''}{nc} = \frac{2\omega n''}{c}.$$
 (2.66)

521

522 Ordinary em radiation comprises randomly distributed directions of polarization for the 523  $\vec{E}$  and  $\vec{B}$  fields. Radiation for which the direction of polarization is constant and the same for all 524 waves is said to be polarized. Reflected em waves are partially polarized in the direction parallel 525 to the reflecting surface, the extent of polarization depending on the angle of incidence. 526 Polaroid® sun glasses are polarized in the vertical direction and therefore more strongly 527 attenuate reflected waves. Reflected em waves are fully polarized at the Brewster incident angle. 528

#### 529 2.2.7 Local Electric Fields

530 The electric field inside a dielectric medium is not equal to the applied field because of 531 electrostatic screening by the medium. This is a complicated problem that is well described in 532 Chapter One of ref. [3] (by N. E. Hill) and has been considered by Onsager [4], Kirkwood [5], 533 and Frohlich [6]. The complexity is exemplified by the Kirkwood relation between the isolated 534 molecular dipole moment  $\mu_g$  observed in the gas phase and the relative permittivity  $\varepsilon_0^E$ 

535

536 
$$\frac{4\pi Ng \mu_g^2}{9k_B T V e_0} = \frac{\left(\varepsilon_0^E - \varepsilon_\infty^E\right) \left(2\varepsilon_0^E + \varepsilon_\infty^E\right)}{\varepsilon_0^E \left(\varepsilon_\infty^E + 2\right)},$$
(2.67)

537

where  $\varepsilon_{\infty}^{E}$  is the limiting high frequency relative permittivity that for a pure dielectric equals the square of the (limiting low frequency) refractive index  $n^2$ , N is the number of dipoles in a volume V, and g is a correlation factor that corrects for nonrandom orientations of surrounding dipoles caused by direction dependent intermolecular forces. The latter is in principle calculable: 542

543 
$$g = 1 + \sum_{i \neq j}^{N} \left\langle \cos\left(\theta_{ij}\right) \right\rangle$$
(2.68)

544

545 where the averaged cosine  $\langle \cos(\theta_{ij}) \rangle$  of the angle  $\theta_{ij}$  between dipoles  $\mu_i$  and  $\mu_j$  can be 546 computed for specific orientation geometries.

547 The treatment of local field effects on the kinetics of dipole relaxation is even more

intricate because the reaction field produced by polarization of the dielectric medium by the embedded dipole is in general out of phase with the applied field. These effects have been discussed by Mountain [7]. A particularly important effect for relaxation phenomenology is that a single macroscopic dielectric relaxation time corresponds to two microscopic times. After a heated debate in the literature the accepted microscopic dipole correlation function is the Fatuzzo and Mason [8] expression

554

 $\varphi(t) = \left(1 + \frac{\varepsilon_{\infty}}{2\varepsilon_{0}}\right)^{-1} \left[\exp\left(-\frac{t}{\tau_{E}}\right) + \left(\frac{\varepsilon_{\infty}}{2\varepsilon_{0}}\right)\exp\left(-\frac{\varepsilon_{0}}{\varepsilon_{\infty}}\frac{t}{\tau_{E}}\right)\right]$   $= \left(1 + \frac{\varepsilon_{\infty}}{2\varepsilon_{0}}\right)^{-1} \left[\exp\left(-\frac{t}{\tau_{E}}\right) + \left(\frac{\varepsilon_{\infty}}{2\varepsilon_{0}}\right)\exp\left(-\frac{t}{\tau_{D}}\right)\right]$ (2.69)

556

where  $\tau_E$  and  $\tau_D$  are again the relaxation times for polarization at constant *E* and *D* respectively. Fulton [9] has given a detailed discussion of this subject in which he deduced that the longitudinal part of polarization relaxes with a time constant  $\tau_D$  and that the transverse component relaxes with a time constant  $\tau_E$ . Electrical relaxation is therefore discussed later in this chapter in two parts - dielectric relaxation and conductivity relaxation.

563 2.2.8 Circuits

564 There are the four fundamental elements in analog passive circuits: resistance R; 565 capacitance C; self inductance L; mutual inductance M.

- 567 2.2.8.1 Simple Circuits
- 568 *Resistances in Series and in Parallel*

For resistances  $R_s$  connected in series, the same current  $I_s$  must pass through each and the sum of the voltages across each resistor equals the applied voltage is. Thus  $V = \sum V_i = IR_s = I \sum R_i$  and the equivalent series resistance is

573 
$$R_s = \sum R_i$$
. (2.70)

574

572

566

For resistances  $R_p$  connected in parallel the same voltage *V* must occur across each and the total current *I* through the parallel circuit is the sum of the currents through each:  $I = \sum I_i = \sum V/R_i$  and the equivalent parallel resistance  $R_p$  is given by 578

579 
$$1/R_p = \sum 1/R_i$$
. (2.71)

- 580
- 581

### Page 18 of 61

582 *Capacitances in Series and in Parallel* 

583 Capacitance *C* is defined as  $C \equiv q/V$ , where *V* is the voltage across the capacitor and 584  $\pm q$  are the charges on each of its ends. For capacitances  $C_i$  connected in parallel the same voltage 585 *V* must occur across each and the total charge *q* on each side of the equivalent parallel 586 capacitance  $C_p$  must equal the sum of charges  $q_i$  on each component. Thus  $q = C_p V = V \sum_i C_i$  and

587 the equivalent parallel capacitance  $C_p$  is given by

589 
$$C_p = \sum_i C_i$$
. (2.72)

590

For capacitances connected in series the total voltage V across the series circuit equals the sum of voltages across each capacitor. The magnitude of the charges q on each must be the same (since no charge separation can occur across the short circuit joining them) so that  $V = q/C_s = \sum_i V_i = \sum_i q/C_i$  and the equivalent series capacitance  $C_s$  is given by

595

596 
$$\frac{1}{C_s} = \sum_i \frac{1}{C_i}$$
. (2.73)

597

## 598 Inductances in Series and in Parallel

599 The self-inductance *L* is defined as  $L \equiv V / (dI / dt)$  where *V* is the voltage across the 600 device and *I* is the current through it. Since *V* is in the numerator and *I* is in the denominator *L* 601 is an impedance akin to *R*. Impedances add in series so the equivalent series inductance is

$$603 L_s = \sum_i L_i (2.74)$$

604

606

602

and since admittances add in parallel the equivalent parallel inductance is

607 
$$\frac{1}{L_s} = \sum_i \frac{1}{L_i}$$
 (2.75)

608

The mutual inductance M of a device is defined as  $M \equiv V_2/(dI_1/dt)$ , where  $V_2$  is the voltage induced on one side of the device by a time varying current  $I_1$  in the other. Mutual inductances are usually insignificant in relaxation instrumentation since they only occur in analog instruments that use transformers that are rarely (never?) used now. Rearrangement of the definition of M yields

614

615 
$$V_2 = M(dI_1/dt),$$
 (2.76)

so that  $V_2$  is smaller at lower frequencies when  $dI_1/dt$  is smaller. This is why transformer arm 617 618 (essentially ac Wheatstone) bridges were useless at low frequencies.

619

#### 620 Combined Series and Parallel Elements

621 Consider two examples of a general circuit in which an element  $Z_1$  is in parallel with a series combination of two elements  $Z_2$  and  $Z_3$ . If these elements are resistances  $R_1$ ,  $R_2$  and  $R_3$  then 622 623  $R_{23} = R_2 + R_3$  and

624

625 
$$\frac{1}{R_{equiv}} = \frac{1}{R_1} + \frac{1}{R_2 + R_3} = \frac{R_1 + R_2 + R_3}{R_1 (R_2 + R_3)}$$
(2.77)

626

627 or 628

629 
$$R_{equiv} = \frac{R_1 \left( R_2 + R_3 \right)}{R_1 + R_2 + R_3}.$$
 (2.78)

630

631 If these elements are capacitances  $C_1$ , then  $C_2$ and  $C_3$  $1/C_{23} = 1/C_2 + 1/C_3 \Longrightarrow C_{23} = C_2C_3/(C_2 + C_3)$  and 632 633

634 
$$C_{equiv} = C_1 + C_{23} = C_1 + \frac{C_2 C_3}{C_2 + C_3} = \frac{C_1 C_2 + C_2 C_3 + C_3 C_1}{C_2 + C_3}.$$
 (2.79)

635

#### 636 2.2.8.2 AC Circuits

If the applied voltage is  $V(t) = V_0 \cos(\omega t) = \operatorname{Re}[V_0 \exp(-i\omega t)]$  the average voltage over 637 one period is zero but the ac power is not. Equation (2.34) indicates that power is determined by 638 the averages of  $I^2$  and  $V^2$  that are both proportional to the averages of  $\sin^2(\omega t)$  or  $\cos^2(\omega t)$  over 639 one cycle that are both equal to  $\frac{1}{2}$ . Thus 640

641

$$642 \qquad P_{average} = \Big($$

 $(V_0^2/2)R = I_0^2 R/2.$ (2.80)

643

644 The ac power dissipation is therefore given by the same relation for DC power dissipation if the maximum ac voltage  $(V_0)$  and current  $(I_0)$  are replaced by  $V_0/\sqrt{2}$  and  $I_0/\sqrt{2}$  respectively. The 645 latter are referred to as rms (root mean square) voltages and currents. Electrical outlet ac voltages 646 such as 120V in North America are given as rms values; the peak voltage in North America is 647 therefore  $(120V)(2)^{1/2} = 170V$ . 648

AC impedances  $Z^*(i\omega)$  are defined as  $V^*(i\omega)/I^*(i\omega)$  and ac admittances  $A^*(i\omega)$ 649 as  $I^*(i\omega)/V^*(i\omega)$ . The imaginary components of  $A^*(i\omega)$  and  $Z^*(i\omega)$  are referred to as 650 651 reactances, and as shown below do not dissipate power.



Page 20 of 61

Resistances For a voltage  $V = V_0 \exp(-i\omega t)$  applied across a resistance *R* the current is 

656 
$$I_{R}(i\omega t) = \frac{V(i\omega t)}{R} = \frac{V_{0}}{R} \exp(-i\omega t) = V_{0}G \exp(-i\omega t)$$
(2.81)  
657 so that the impedance is

659 
$$Z_{R}^{*}(i\omega t) = \frac{V^{*}(i\omega t)}{I^{*}(i\omega t)} = \frac{V_{0}\exp(-i\omega t)}{(V_{0}/R)\exp(-i\omega t)} = R$$
(2.82)

and the admittance  $A_R^*(i\omega t) = 1/Z_R^*(i\omega t) = G$  where G is the conductance. Both R and G are real and independent of frequency. 

*Capacitances* 

For a capacitance C the current is 

667 
$$I_{C}(i\omega t) = \frac{dq(\omega t)}{dt} = C \frac{dV(i\omega t)}{dt} = V_{0} \Big[ -i\omega C \exp(-i\omega t) \Big]$$
(2.83)

and the capacitive impedance is

671 
$$Z_{C}^{*}(i\omega t) = \frac{V^{*}(i\omega t)}{I_{C}^{*}(i\omega t)} = \frac{V_{0}\exp(-i\omega t)}{V_{0}\left[-i\omega\exp(-i\omega t)\right]} = \frac{1}{-i\omega C} = \frac{i}{\omega C}$$
(2.84)

and the capacitive admittance is

$$675 \qquad A_C^*(i\omega t) = -i\omega C. \tag{2.85}$$

The capacitive admittance and admittance are therefore frequency dependent and imaginary (thus a reactance). Power dissipation per cycle in a capacitance is given by

$$P_{C}(t) = \langle V_{C}(t)I_{C}(t) \rangle = \langle [V_{0}\exp(-i\omega t)]V_{0}[-i\omega C_{p}\exp(-i\omega t)] \rangle = -V_{0}^{2}\omega C_{p} \langle \exp(-2i\omega t) \rangle$$

$$680 = \langle -V_{0}^{2}\omega C_{p}[\cos(-2\omega t)-i\sin(-2\omega t)] \rangle$$

$$= \langle -V_{0}^{2}\omega C_{p}[\cos(-2\omega t)] \rangle + \langle iV_{0}^{2}\omega C_{p}\sin(-2\omega t) \rangle = 0$$

$$(2.86)$$

because the averages of both  $\cos(2\omega t)$  and  $\sin(2\omega t)$  over one cycle are zero. The capacitive impedance is therefore not a resistance if "resistance" is taken to imply power dissipation. This is the why an inductive or capacitive impedance is not considered to be an "ac resistance". For the phase convention adopted here the reactance is capacitive if the imaginary part of the complex admittance is negative and is inductive if the imaginary part of the complex admittance is positive.

688

689 Inductances

For a self-inductance *L* the current is

692 
$$I_{L}(\omega t) = \int \left(\frac{V}{L}\right) dt = \int \left(\frac{V_{0} \exp(-i\omega t)}{L}\right) dt = \left(\frac{V_{0}}{L}\right) \frac{\exp(-i\omega t)}{-i\omega}$$
(2.87)

693

695

694 so that inductive impedance is

696  $Z_{L}^{*}(i\omega t) = \frac{V^{*}(i\omega t)}{I_{L}^{*}(i\omega t)} = -i\omega L$ (2.88)

697

698 and the inductive admittance is

699

700 
$$A_L^*(i\omega t) = \frac{1}{-i\omega L} = \frac{i}{\omega L}.$$
 (2.89)

701

The inductive reactance is therefore also imaginary and frequency dependent. Power dissipation
 in an inductance is given by

$$P_{L}(t) = \langle V_{L}(t) I_{L}(t) \rangle = \left\langle \left[ V_{0} \exp(-i\omega t) \right] \left( \frac{V_{0}}{L} \right) \frac{\exp(-i\omega t)}{-i\omega} \right\rangle$$

$$= -\frac{V_{0}^{2}}{-i\omega L} \left\langle \exp(-2i\omega t) \right\rangle = \frac{V_{0}^{2}}{i\omega L} \left\langle \exp(-2i\omega t) \right\rangle = 0.$$
(2.90)

706

Thus the power dissipated by a pure inductance is zero just like that of a capacitance ("pure"meaning negligible resistance).

- 709
- 710 Parallel Resistance and Capacitance

711 Consider a voltage  $V = V_0 \cos(\omega t)$  applied across a resistance  $R_p$  in parallel with a 712 capacitance  $C_p$ . The current  $I_R$  through the resistance is

714 
$$I_{R} = \frac{V}{R_{p}} = \frac{V_{0}\cos(\omega t)}{R_{p}} = V_{0}\cos(\omega t)G_{p} = \operatorname{Re}\left[V_{0}G_{p}\exp(-i\omega t)\right]$$
(2.91)

715

717

716 where  $G_p = 1/R_p$  is the conductance. The current through the capacitance  $I_C$  is

718 
$$I_{C} = \frac{dq_{C}}{dt} = C_{p} \frac{dV}{dt} = -V_{0}\omega C_{p} \sin(\omega t)$$

$$= -V_{0}\omega C_{p} \cos(\omega t - \pi/2) \operatorname{Re}\left[-iV_{0}\omega C_{p} \exp(-i\omega t)\right]$$
(2.92)

719

where  $q_C$  is the charge on the capacitor. Equation (2.92) implies that the sinusoidal (displacement) current  $I_C$  lags the applied voltage by  $\pi/2$  radians because  $\sin(\omega t) = \cos(\omega t - \pi/2)$ . The total current through the parallel  $R_p C_p$  circuit is

$$I = I_{R} + I_{C} = V_{0}G_{p}\cos(\omega t) - V_{0}\omega C_{p}\sin(\omega t)$$

$$= \operatorname{Re}\left[V_{0}G_{p}\exp(-i\omega t)\right] + \operatorname{Re}\left[-iV_{0}\omega C_{p}\exp(-i\omega t)\right]$$

$$= \operatorname{Re}\left\{V_{0}\left[G_{p} - i\omega C_{p}\right]\exp(-i\omega t)\right\}.$$
(2.93)

The phase relations for the current are therefore conveniently expressed by defining the parallel combination of resistance and capacitance as a complex admittance  $A^*$ 

$$726 \qquad A^* = G_p - i\omega C_p, \qquad (2.94)$$

727 or as a complex impedance  $Z^*$ 

728 
$$Z^* = 1/A^* = \frac{1}{G_p - i\omega C_p} = \frac{G_p}{G_p^2 + \omega^2 C_p^2} + \frac{i\omega C_p}{G_p^2 + \omega^2 C_p^2}.$$
 (2.95)

729 The complex capacitance is

730 
$$C^* = \frac{A^*}{-i\omega} = C_p + \frac{iG_p}{\omega}$$
(2.96)

and the complex electric modulus is

732 
$$M^{*}(i\omega) = 1/C^{*}(i\omega) = i\omega Z^{*}(i\omega).$$
 (2.97)

733 Equation (2.95) is equivalent to

734 
$$Z^* = \frac{R_p}{1 + \omega^2 \tau_D^2} + \frac{iR_p \omega \tau_D}{1 + \omega^2 \tau_D^2}$$
 (2.98)

735 where

$$\tau_D = R_p C_p \tag{2.99}$$

is the Maxwell relaxation time (the reason for the subscript D is given below).

When normalized by the cell constant *k* (dimensions m<sup>-1</sup>) the quantities  $A^*$ ,  $Z^*$  and  $C^*$ become respectively the complex conductivity  $\sigma^* = kA^*$ , complex resistivity  $\rho^* = Z^*/k$ , and complex relative permittivity  $\varepsilon^* = kC^*/e_0 = C^*/C_0$  where  $C_0$  is the capacitance of the measuring cell in a vacuum (usually equated to that in air).

742 The reciprocal of 
$$\mathcal{E}^*(i\omega)$$
 is the complex electric modulus

Page 23 of 61

744 
$$M^*(i\omega) = \frac{1}{\varepsilon^*(i\omega)}$$
(2.100)

745

746 so that 747

748 
$$M' = \frac{\varepsilon'}{\varepsilon'^2 + \varepsilon''^2}; M'' = \frac{\varepsilon''}{\varepsilon'^2 + \varepsilon''^2}.$$
 (2.101)

749

750Series Resistance and Capacitance751For a resistance  $R_s$  in series with a capacitance  $C_s$ 752

753 
$$Z^*(i\omega) = R_s + \frac{1}{i\omega C_s} = R_s - \frac{i}{\omega C_s} = R_s \left(\frac{\omega \tau_E - i}{\omega \tau_E}\right), \qquad (2.102)$$

754

755 
$$A^{*}(i\omega) = \frac{R_{s}}{1 + \omega^{2}R_{s}^{2}C_{s}^{2}} + \frac{i\omega R_{s}^{2}C_{s}}{1 + \omega^{2}R_{s}^{2}C_{s}^{2}} = \frac{R_{s}}{1 + \omega^{2}\tau_{E}^{2}} + \frac{i\omega R_{s}\tau_{E}}{1 + \omega^{2}\tau_{E}^{2}},$$
(2.103)

757 
$$C^{*}(i\omega) = \frac{A^{*}(i\omega)}{-i\omega} = C_{s} \left( \frac{1 - i\omega R_{s} C_{s}}{1 + \omega^{2} R_{s}^{2} C_{s}^{2}} \right) = C_{s} \left( \frac{1}{1 + \omega^{2} \tau_{E}^{2}} - \frac{i\omega \tau_{E}}{1 + \omega^{2} \tau_{E}^{2}} \right),$$
(2.104)

758

$$M^{*}(i\omega) = \frac{1}{C^{*}(i\omega)} = \frac{-i\omega}{A^{*}(i\omega)} = -i\omega Z^{*}(i\omega) = -i\omega \left[ R_{s} - \frac{i}{\omega C_{s}} = R_{s} \left( \frac{\omega \tau_{E} - i}{\omega \tau_{E}} \right) \right]$$

$$= \frac{-R_{s}}{\tau_{E}} \left( 1 + i\omega \tau_{E} \right)$$
(2.105)

760

761 where  $\tau_E \equiv R_s C_s$  and is not generally equal to  $\tau_D \equiv R_p C_p$ .

The relations between the four response functions are conveniently summarized by [1,10]  $a^*(i\alpha) \longrightarrow 1/M^*(i\alpha)$ 

764

$$\begin{array}{cccc}
\varepsilon^{*}(i\omega) & \Leftrightarrow & 1/M^{*}(i\omega) \\
\uparrow & \uparrow & & & \\
\sigma^{*}(i\omega)/(ie_{0}\omega) & \Leftrightarrow & ie_{0}\omega/\rho^{*}(i\omega)
\end{array}$$
(2.106)

765

766 2.2.8.3 Experimental Factors

767 *Cable Effects* 

768 Cable impedances can be analyzed using transmission line techniques that invoke an 769 infinite number of  $\{L, C\}$  components. One line of the cable is considered to be a series of 770 inductances L and the other line as a zero impedance wire, with capacitances C connecting the

#### Page 24 of 61

771 two between every pair of inductances. In the limit of an infinite number of inductance and capacitance elements the cable impedance is  $Z_{cable} = (L/C)^{1/2}$  and is real and constant. Coaxial 772 cables are made so that C is 30 pF/ft and L is 0.075  $\mu$ H/ft so 773 that  $Z_{cable} = (7.5 \times 10^{-8} H / 3.0 \times 10^{-11})^{1/2} = 50\Omega$ . Thus a short cable with a 50  $\Omega$  resistor across it looks 774 like an infinitely long cable and a 50  $\Omega$  load on the cable has an ideal impedance match for 775 776 maximum power transfer (see electrical engineering texts). Such a cable will also behave as an 777 inductor if short circuited so that for a high conductivity attached sample resonance effects may 778 be significant. 779

780 *Electrode Polarization* 

781 This occurs for two and three terminal measurements when charge transfer does not 782 occur between an electrode and the sample material, i.e. when the applied voltage is less than the 783 decomposition potential of the sample (four terminal measurements are immune to this but they 784 do not produce reliable capacitance data and require separate sample preparation). In this case 785 the contact can be approximated as a large capacitance  $C_s$  in series with the sample [11-13]. If the amplitude of the applied potential is too large (above the decomposition potential of the 786 787 electrolyte) a Faradaic impedance [14, 15] will also occur in parallel with this capacitance [16] 788 that can sometimes be approximated as a Warburg impedance.

A series capacitance does not affect  $M''(\omega)$  and simply adds  $1/C_s$  to  $M'(\omega)$ : the total impedance  $Z_{total}^*(i\omega)$  of the sample impedance  $Z^*(i\omega)$  and  $C_s$  is  $Z_{total}^*(i\omega) = Z^*(i\omega) + 1/i\omega C_s$  so that 792

793 
$$M^{*}(i\omega) = i\omega Z^{*}_{total} = i\omega Z^{*}(i\omega) + 1/C_{s}$$
. (2.107)  
794

It is a considerable advantage of the electric modulus function that  $M''(\omega)$  is unaffected by electrode polarization and other high capacitance phenomena. This is exploited in some of the methods of data analysis discussed below but it is noted that this advantage is not shared by the imaginary component of the resistivity  $\rho''$  because

799

800 
$$\lim_{\omega \to 0} \rho''(\omega) \propto \lim_{\omega \to 0} \left( \frac{1}{k \, \omega C_s} \right) = \infty.$$
(2.108)

801

The low frequency behavior of  $\rho'$  can be useful (see below). Electrode polarization can make the direct determination of the low frequency quantities  $\varepsilon_0$  and  $\sigma_0$  difficult and sometimes impossible because it increases  $\varepsilon'$  above  $\varepsilon_0$  at low frequencies and, usually at lower frequencies, decreases  $\sigma'$  to below  $\sigma_0$ . Overlap between bulk relaxations and these two electrode polarization effects often prevents the observation of limiting low frequency plateaus in  $\varepsilon'(\omega)$  and/or  $\sigma'(\omega)$ . Although relaxation of electrode polarization occurs at lower frequencies than the bulk relaxation,

Page 25 of 61

809

810 
$$\tau_{electrode} = \frac{\epsilon_0 C_s}{C_0 \sigma_0} \Longrightarrow \frac{\epsilon_0 C_p}{C_0 \sigma_0} = \tau_D, \qquad (2.109)$$

811

the magnitude of the polarization dispersion can be very large [proportional to  $(C_s - C_p) \approx C_s$ ] 812 and its high frequency tail can extend well into the bulk relaxation region. This phenomenon is 813 illustrated by the following representative average circuit quantities: a parallel capacitance 814  $C_p = 10 \,\mathrm{pF}$  and parallel resistance  $R_p = 10^7 \,\mathrm{ohm}$  in series with a polarization capacitance of 815  $C_s = 10^4 \text{ pF}$ . Because both  $R_p$  and  $C_p$  will have distributions in a typical electrolyte there will be 816 dispersions in both  $\varepsilon'$  and  $\sigma'$ . The dispersion is centered around  $\omega \approx 1/(R_p C_p) = 10^4 \,\mathrm{s}^{-1}$  and 817 the low frequency plateau in  $\varepsilon'$  would normally be seen at ca.  $\omega \approx 10^2 \text{ s}^{-1}$ , but this is dwarfed by 818 the polarization capacitance at that frequency,  $C_{pol}(\omega >> (R_p C_s)^{-1}) = C_s / (\omega^2 R_p^2 C_s^2) = 100 \, \text{pF}$ , 819 an order of magnitude higher than  $C_p$ . On the other hand, the low frequency dispersion in 820 polarization has 821 conductivity due to barely begun at  $\omega = 10^2$ :  $\sigma_{ele} / \sigma_0 = \omega^2 \tau_{ele}^2 / (1 + \omega^2 \tau_{ele}^2) = 0.99$  for  $\omega \tau_{ele} = \omega R_p C_s = (10^2) (10^{-1}) = 10$ , where the fact 822 823 that the limiting high frequency conductivity for the Debye-like relaxation of electrode 824 polarization is  $\sigma_0$ :

825

826 
$$\lim_{\omega \tau_{ele} \to \infty} \sigma_{ele} = \frac{\left(\varepsilon_0 - \varepsilon_{\infty}\right)_{ele} \mathbf{e}_0}{\tau_E} = \frac{\left(\varepsilon_0 - \varepsilon_{\infty}\right)_{ele} \mathbf{e}_0 \varepsilon_{\infty}}{\tau_D \varepsilon_0} = \frac{\left(\varepsilon_0 - \varepsilon_{\infty}\right)_{ele} \sigma_0}{\varepsilon_0} \approx \sigma_0 \text{ for } \varepsilon_{0,ele} >> \varepsilon_{\infty,ele}$$
(2.110)

827

Effects similar to electrode polarization can arise from other causes, such as poor electrode contact where a capacitance due to air gaps occurs in parallel with a resistance at the contact areas. Poor contacts have been shown to give spurious dielectric losses in un-doped alkali halides [17], and is suspected to be responsible for the poor reproducibility of other dielectric data for alkali halides [18]. Space charge effects can also produce a series capacitance at the electrode [19,20].

834

835 2.3 Dielectric Relaxation

An excellent resource for dielectric relaxation that is ref. [3], particularly Chapter One by N. E. Hill. An excellent review of dielectric relaxation phenomena in supercooled and glassy materials is given by Richert [21] that also includes references to modern measurement technology.

840

841 2.3.1 Frequency Domain

842 2.3.1.1 Dipole Rotation

843 A freely rotating dipole in a sinusoidally varying electric field with an angular frequency 844  $\omega$  low enough that the dipole can keep up with the field behaves as a pure capacitance  $C_{pure}$ .

845 The current then lags the field by  $\pi/2$  radians and the complex admittance is

846

847  $A^* = i\omega C_{pure}.$ 

848

849 If the dipole cannot keep up with the field because of friction with its environment it will lag by 850 an additional angle  $\delta$  and a component of the current appears in phase with the voltage and is 851 measured as a resistance. Thus eq. (2.92) is replaced by

(2.111)

852

$$I_{c} = -V_{0}\omega C_{p}\cos(\omega t - \pi/2 - \delta)$$

$$853 = -V_{0}\omega C_{p}\left[\cos(\omega t - \pi/2)\cos\delta + \sin(\omega t - \pi/2)\sin\delta\right]$$

$$= -V_{0}\omega C_{p}\left[\sin(\omega t)\cos\delta - \cos(\omega t)\sin\delta\right]$$

$$(2.112)$$

854

and the term  $+V_0 \omega C_p \cos(\omega t) \sin \delta$  in eq. (2.112) is indeed in phase with the applied voltage  $V = +V_0 \cos(\omega t)$ . Note that this in-phase component is zero when  $\delta = 0$ . Comparing eq. (2.112) with eqs. (2.93) and (2.94) reveals that

859 
$$A^* = \omega C_{pure} \sin \delta + i\omega C_{pure} \cos \delta$$
(2.113)

860 861 And

863 
$$C^* = C' - iC'' = C_{pure} \cos \delta - iC_{pure} \sin \delta$$
(2.114)

864 865

so that

and

866

862

867 
$$G_p(\text{effective}) = \omega C_{pure} \sin \delta$$
 (2.115)

868 869

870

871 
$$C_p(\text{effective}) = C_{pure} \cos \delta$$
. (2.116)

Note that at low frequencies when the lag angle  $\delta$  tends to zero the effective capacitance equals  $C_{pure}$  and  $G_p = 0$  as must be. When normalized by the geometric capacitance associated with the cell constant k,  $C_0 = e_0 / k$  where  $e_0$  is the vacuum permittivity  $8.854 \times 10^{-12}$  F m<sup>-1</sup>, the complex capacitance becomes the complex permittivity,  $\varepsilon^* = C^*/C_0$  so that

$$\begin{array}{l} 876\\ 877\\ \varepsilon^* = \varepsilon' - i\varepsilon'' \end{array} \tag{2.117}$$

878

879 where 880

Page 27 of 61

881 
$$\varepsilon' = \frac{C_p}{C_0} (\varepsilon_0 - \varepsilon_\infty) \cos(\delta) + \varepsilon_\infty, \qquad (2.118)$$

882 
$$\varepsilon'' = \frac{G_p}{\omega \cdot C_0} = \frac{\sigma}{e_0 \cdot \omega} = \frac{C_p}{C_0} (\varepsilon_0 - \varepsilon_\infty) \sin(\delta), \qquad (2.119)$$

883

884 and

885

886 
$$\tan \delta = \frac{\varepsilon''}{\varepsilon'} = \frac{G_p}{\omega C_p}.$$
 (2.120)

887

Note that  $\tan \delta$  is independent of the geometric capacitance  $C_0$  and has the same frequency dependence as  $\varepsilon''$  but with a retardation time of  $\left(\varepsilon_{\infty}^{E}/\varepsilon_{0}^{E}\right)^{1/2} \tau_{E}$  rather than  $\tau_{E}$ . Equations (2.113) and (2.114) imply

$$891 \qquad A^* = i\omega C_0 \varepsilon^* \tag{2.121}$$

$$893 \qquad \sigma^* = kA^* = i\omega \mathbf{e}_0 \varepsilon^* \tag{2.122}$$

895 
$$\rho^* = \frac{1}{\sigma^*} = \frac{1}{i\omega e_0 \varepsilon^*}$$
(2.123)

896 The complex electric modulus  $M^*$  is defined as the reciprocal of  $\varepsilon^*$ : 897  $M^* = 1/\varepsilon^*$  (2.124)

899

900 
$$M^* = i\omega C_0 Z^* = i\omega e_0 \rho^*$$
 (2.125)

901

902 The functions  $\sigma^*$ ,  $\varepsilon^*$ ,  $\rho^*$  and  $M^*$  are all analytical and their components all conform to the 903 Cauchy-Riemann and Kronig-Kramers equations.

For a single relaxation time the (Debye) functions  $\varepsilon^*(i\omega)$ ,  $\varepsilon'(\omega)$  and  $\varepsilon''(\omega)$  for dielectric relaxation are

906 
$$\varepsilon^*(i\omega) = \varepsilon_{\infty}^E + \frac{(\varepsilon_0^E - \varepsilon_{\infty}^E)}{1 + i\omega\tau_E},$$
 (2.126)

907 
$$\varepsilon'(\omega) = \varepsilon_{\infty}^{E} + \frac{\left(\varepsilon_{0}^{E} - \varepsilon_{\infty}^{E}\right)}{1 + \omega^{2}\tau_{E}^{2}},$$
(2.127)

908 and

909 
$$\varepsilon''(\omega) = \frac{\left(\varepsilon_0^E - \varepsilon_\infty^E\right)\omega\tau_E}{1 + \omega^2 \tau_E^2},$$
(2.128)

#### Page 28 of 61

910 where  $\varepsilon_0^E$  and  $\varepsilon_{\infty}^E$  are defined in §2.1.1 as the limiting low and high frequency limits of  $\varepsilon'(\omega)$ 

911 respectively. Equations (2.127) and (2.128) yield a complex plane plot of  $\varepsilon''$  vs  $\varepsilon'$  that is a 912 semicircle centered on the real axis at  $\varepsilon' = (\varepsilon_0^E + \varepsilon_{\infty}^E)/2$ . This is found by eliminating  $\omega \tau_E$ 

913 between equations (2.127) and (2.128).

914 The corresponding Debye functions for  $\sigma'(\omega)$  and  $\sigma''(\omega)$  are

915 
$$\sigma'(\omega) = e_0 \omega \varepsilon''(\omega) = \frac{e_0 \left(\varepsilon_0^E - \varepsilon_\infty^E\right) \omega^2 \tau_E}{1 + \omega^2 \tau_E^2}$$
(2.129)

916 and

917 
$$\sigma''(\omega) = \mathbf{e}_0 \omega \varepsilon_{\infty}^E + \frac{\mathbf{e}_0 \omega \left(\varepsilon_0^E - \varepsilon_{\infty}^E\right)}{1 + \omega^2 \tau_E^2}.$$
 (2.130)

918

919 Thus the real part of the conductivity of a Debye dielectric increases from zero at low 920 frequencies to a high frequency limit of

921

922 
$$\sigma_{\infty} = \lim_{\omega \to \infty} \sigma'(\omega) = e_0 \left( \varepsilon_0^E - \varepsilon_{\infty}^E \right) / \tau_E$$
(2.131)

923

924 and the imaginary part diverges at high frequencies. Derivations of the Debye expressions for 925  $M'(\omega)$  and  $M''(\omega)$  are instructive and straightforward but tedious – they are given in Appendix 926 2.1. The results are

(2.132)

927 928  $M'(\omega) = M_0^D + \frac{\left(M_\infty^D - M_0^D\right)\omega^2 \tau_D^2}{1 + \omega^2 \tau_D^2}$ 

929 and

930 
$$M''(\omega) = \frac{\left(M_{\infty}^{D} - M_{0}^{D}\right)\omega\tau_{D}}{1 + \omega^{2}\tau_{D}^{2}},$$
(2.133)

931

932 where  $M_0^D = 1/\varepsilon_0^D$ ,  $M_\infty^D = 1/\varepsilon_\infty^D$ , and  $(\varepsilon_\infty^D / \varepsilon_0^D)\tau_E = \tau_D$ .

If a limiting low frequency conductivity  $\sigma_0$  is present that is not physically related to the dielectric loss process (e.g. ionic conductivity in a dilute aqueous solution), it must be subtracted from the measured conductivity before the dielectric loss is calculated from eq. (2.128). Otherwise the limiting low frequency dielectric loss  $\lim_{\omega \to 0} \varepsilon'' \to 0$  will be masked by the rapid rise

- 937 from the conductivity contribution
- 938

939 
$$\lim_{\omega \to 0} \varepsilon'' = \lim_{\omega \to 0} \frac{\sigma_0}{e_0 \omega} \to \infty.$$
(2.134)

940

It has been argued that this subtraction is physically meaningful only if the conductivity is unrelated to the dielectric loss process (as in the aqueous solutions mentioned above, for example). If the dielectric loss peak correlates with  $\sigma_0$  as occurs in alkali silicate glasses [22-28] then the subtraction of  $\sigma_0$  can be regarded as artificial and other methods of data analysis are preferred (although this position is not universally accepted). This is the principle reason for not using the complex permittivity in analyzing highly conducting materials and is the subject of \$2.4.

948 If the decay function is nonexponential dielectric relaxation can be described in terms of 949 a distribution of retardation times  $g(\ln \tau_E)$  defined by the relations

950

951 
$$\phi_E(t) = \int_{-\infty}^{+\infty} g\left(\ln \tau_E\right) \exp\left(-\frac{t}{\tau_E}\right) d\ln \tau_E$$
(2.135)

952 and

953 
$$\int_{-\infty}^{\infty} g\left(\ln \tau_E\right) d\ln \tau_E = 1$$
(2.136)

954

955 so that eq. (2.126) generalizes to 956

957 
$$\varepsilon^* - \varepsilon^E_{\infty} = \left(\varepsilon^E_0 - \varepsilon^E_{\infty}\right) \int_{-\infty}^{+\infty} \frac{g\left(\ln \tau_E\right)}{1 + i\omega\tau_E} d\ln \tau_E.$$
(2.137)

958

959 The generalization of eqs. (2.127) and (2.128) are 960

961 
$$\varepsilon'(\omega) = \varepsilon_{\infty}^{E} + \left(\varepsilon_{0}^{E} - \varepsilon_{\infty}^{E}\right) \left[ \int_{-\infty}^{-\infty} g\left(\ln\tau_{E}\right) \frac{1}{1 + \omega^{2}\tau_{E}^{2}} \right] d\ln\tau_{E} = \varepsilon_{\infty}^{E} + \left(\varepsilon_{0}^{E} - \varepsilon_{\infty}^{E}\right) \left\langle \frac{\omega\tau_{E}}{1 + \omega^{2}\tau_{E}^{2}} \right\rangle$$
(2.138)

962 and

963 
$$\varepsilon''(\omega) = \left(\varepsilon_0^E - \varepsilon_\infty^E\right) \int_{-\infty}^{-\infty} g\left(\ln \tau_E\right) \frac{\omega \tau_E}{1 + \omega^2 \tau_E^2} d\ln \tau_E = \left(\varepsilon_0^E - \varepsilon_\infty^E\right) \left\langle \frac{\omega \tau_E}{1 + \omega^2 \tau_E^2} \right\rangle.$$
(2.139)

964

966

965 The  $n^{th}$  moments of a distribution function are

967 
$$\left\langle \tau_{E}^{n} \right\rangle = \int_{-\infty}^{+\infty} \tau_{E}^{n} g\left(\ln \tau_{E}\right) d\ln \tau_{E}.$$
 (2.140)

Page 30 of 61

969 If the integral  $\int_{-\infty}^{+\infty} g(\ln \tau_E) d \ln \tau_E$  diverges, as it does for a constant phase angle impedance for 970 example,  $g(\ln \tau_E)$  is not renormalizable and a constant phase angle impedance can therefore be 971 valid only over a limited range in relaxation times. In terms of  $\phi(t)$  the moments are

972

973 
$$\left\langle \tau_{E}^{n} \right\rangle = \frac{1}{\Gamma(\omega)} \int_{0}^{+\infty} t^{n-1} \phi(t) dt$$
 (2.141)  
974

975 and

976

977 
$$\left\langle \tau_{E}^{-n} \right\rangle = \left(-1\right)^{n} \left[ \frac{d^{n} \left( \phi_{E} \right)}{dt^{n}} \right]_{t=0}$$
 (2.142)

978

979 2.3.1.2 Ionic Hopping

980 Chapter One of [3] by N. E. Hill discusses the studies of Frohlich [6] and others on the 981 dielectric relaxation consequences of two state models. We select here the Frohlich account of an 982 entity that has only two possible equilibrium positions 1 and 2. The entity could be a molecular 983 dipole or an ion for example. If the transition probabilities between the two positions are  $w_{12}$  and 984  $w_{21}$  when there is no applied field then a Debye relaxation with a single relaxation time  $\tau_E = 1/(w_{12} + w_{21})$  is predicted that has an Arrhenius temperature 985 dependence  $\tau_E = A \exp(\Delta H / RT)$  where the pre-exponential factor A is a weak function of temperature and 986 987  $\Delta H$  is the energy barrier that separates the two positions. As noted by Hill, however, a 988 nonexponential decay function may result from local field effects.

990 2.3.2 Time Domain

991 Consider the case where an electric field *E* is "instantaneously" increased from zero to  $E_0$ 992 across a dielectric sample at time t = t' and kept constant thereafter, i.e.  $E(t) = E_0 h(t')$  where 993 h(t) is the Heaviside function (see eq. (1.327) in Chapter One). The initially randomized dipoles 994 will partially orient themselves over time and the polarization and displacement will both 995 increase (the final average orientation will not be complete because of thermal fluctuations):

989

$$D(t) = D(0) + [D(\infty) - D(0)][1 - \phi_E(t)], \qquad (2.143)$$

998

999 where D(0) and  $D(\infty)$  are the limiting short time (high frequency) and long time (low 1000 frequency) values of D(t) and  $\phi_E(t)$  is the decay function for polarization at constant *E* 1001 corresponding to D(t). The increase of *D* from zero to  $D(\infty)$  is "instantaneous" compared with 1002 dielectric relaxation times (generally no shorter than about  $10^{-11}$  s) and is due to polarization of 1003 molecular electron clouds that occurs roughly on optical time scales.

1004 It is sometimes convenient to approximate the relation between time domain data and

1005  $\varepsilon''(\omega)$  by the Hamon approximation

1006

1007 
$$\varepsilon''(\omega) \approx \left(\varepsilon_0^E - \varepsilon_\infty^E\right) \left(\frac{-d\phi_E}{dt}\right) \left(\frac{5t}{\pi}\right),$$
 (2.144)  
1008

1009 obtained from the simplification that the normalized displacement current is given by

1011 
$$\left(\frac{-d\phi_E}{dt}\right) \sim t^{-n}$$
 (2.145)

1012

1010

1013 No comparably simple relation exists between  $\varepsilon'(\omega)$  and  $\phi(t)$ . Williams, Watt, Dev and North 1014 [29] have shown that for the Williams-Watt [30] decay function 1015

1016 
$$\phi(t) = \exp\left[-\left(\frac{t}{\tau_0}\right)^{\beta}\right]$$
(2.146)

1017

1018 the Hamon approximation is accurate within 1% for  $\omega \tau_0 > 1$  but fails for  $\omega \tau_0 \le 1$  and  $\beta > 0.2$ . 1019 Equation (2.144) therefore offers a high frequency approximation to the frequency domain 1020 Williams-Watt function that cannot be expressed in terms of named functions.

1021 The complex relative permittivity  $\varepsilon^*(\omega)$  is related to the derivative of  $\varepsilon(t)$  by

1022

1023 
$$\varepsilon^*(i\omega) - \varepsilon^E_{\infty} = \left(\varepsilon^E_0 - \varepsilon^E_{\infty}\right) \int_0^{\infty} -\left(\frac{d\phi_E}{dt}\right) \exp(-i\omega t) dt$$
 (2.147)

1024

1025 where  $\varepsilon_0 = D(\infty)/E_0$  and  $\varepsilon_{\infty} = D(0)/E_0$ . In the simplest case  $\phi_E(t)$  is exponential,

1026

1027 
$$\phi_E(t) = \exp\left[-\left(\frac{t}{\tau_E}\right)\right]$$
(2.148)

1028

1031

1029 and insertion of eq. (2.148) into eq. (2.147) yields the Debye equations (2.127) and (2.128) 1030 [Chapter One of ref. 3].

1032 2.3.3 Temperature Domain

1033 In many situations  $\omega$  and  $\tau_E$  are approximately interchangeable variables. Since  $\tau_E$ 1034 often varies strongly with temperature a narrow temperature range can be used as a surrogate for

#### Page 32 of 61

1035 a wide frequency range. The temperature dependence of  $\tau_E$  is approximated over small ranges in 1036 temperature *T* by the Arrhenius relation

1037 
$$\tau = \tau_0 \exp\left(\frac{E_a}{RT}\right),$$
 (2.149)

where  $\tau_0$  is independent of temperature, R is the ideal gas constant, and  $E_a$  is the activation 1038 energy. Thus the variables  $\ln(\omega \tau)$  at constant  $\omega$  and  $E_{a}/RT$  are equivalent for a single 1039 1040 relaxation time dielectric. In this case eq. (2.149) indicates that over the convenient temperature range from liquid nitrogen (77 K) to room temperature (300K) the retardation time can vary over 1041 a very large range. For example  $\tau$  changes by a factor of 10<sup>25</sup> for an activation energy of 50 1042 1043 kJ/mol. The temperature variable is therefore extremely useful for scans of the total relaxation 1044 spectrum and is frequently used for polymers whose relaxation behavior is typically characterized by widely separated and very broad relaxation processes. Activation energies  $E_a$ 1045 are obtained from plots of log frequency  $\ln f$  against the inverse temperature  $1/T_{\text{max}}$  at which  $\varepsilon''$ 1046 1047 or  $\tan \delta$  passes through its maximum:

1048

1049 
$$\left\langle \frac{E_a}{R} \right\rangle = -\left\lfloor \frac{d\ln f}{d\left(1/T\right)} \right\rfloor.$$
 (2.150)

1050

1051 It has been reported [32] that the activation energy obtained in this way is ambiguous because it 1052 depends on whether the derivative is determined in the isothermal frequency domain or in the 1053 temperature domain at constant frequency: the frequency domain plot of  $\ln f_{\text{max}}$  vs. 1/T was found 1054 to be strongly curved whereas the plot of  $\ln f$  vs.  $1/T_{\text{max}}$  was found to be linear.

1055 Although temperature is useful because of its experimental convenience it is not 1056 quantitative because essentially everything changes with temperature. For example the 1057 dispersion  $\left(\varepsilon_0^E - \varepsilon_\infty^E\right)$  can only be estimated because both  $\varepsilon_0^E$  and to a much less extent  $\varepsilon_\infty^E$  are 1058 temperature dependent. The dispersion  $\left(\varepsilon_0^E - \varepsilon_\infty^E\right)$  can be estimated from the relation [33] 1059

1060 
$$\left(\varepsilon_{0}^{E}-\varepsilon_{\infty}^{E}\right)\approx\left(\frac{2}{\pi R}\right)\left\langle\frac{1}{E_{A}}\right\rangle^{-1}\int_{0}^{\infty}\varepsilon''(T)d(1/T)$$
 (2.151)

1061

but this is approximate because of two assumptions in its derivation that must be made for mathematical tractability: (i)  $\left(\varepsilon_{0}^{E} - \varepsilon_{\infty}^{E}\right)$  is independent of temperature [32] and (ii)  $\left\langle E_{a}\right\rangle = \left\langle 1/E_{a}\right\rangle^{-1}$ that is not generally true because of the Schmidt inequality (Chapter One)

1066 
$$\langle E_A \rangle \langle 1/E_A \rangle^{-1} \ge 1.$$
 (2.152)

1067

1068 The approximation is clearly better for smaller temperature ranges. There are two situations 1069 where  $\ln \omega$  and  $E_a/RT$  are not even approximately equivalent: (i) functions for which  $\omega$  and  $\tau_E$  are not invariably multiplied together (for example the conductivity of a Debye dielectric, eq.(2.128)); (ii) distributions of retardation times that change with temperature.

1072 1073

## 2.3.4 Equivalent Circuits

1074 The electrical response for an exponential dielectric decay function, the Debye relations eqs. (2.127) and (2.128) plus any separate conductivity contribution  $\sigma_{E}$ , is simulated by an 1075 equivalent circuit comprising three parallel arms: a capacitance  $C_p$ , a series combination of  $R_s$ 1076 1077 and  $C_s$ , and a resistance  $R_p$ . The relaxation part of the circuit is the series component  $R_s + C_s$ 1078 the parallel resistance  $R_p$  corresponds to the separate conductivity and the parallel capacitance  $C_{p}$  simulates the limiting high frequency permittivity. If for a particular range of frequencies the 1079 equivalent circuit of an experimental sample resembles  $R_s + C_s$  and the frequency range 1080 encompasses  $\omega = 1/(R_s C_s)$  then a dielectric loss peak will be observed in that frequency range. 1081 1082 An example is electrode polarization in a conducting medium that at low frequencies is 1083 approximated by an electrode capacitance in series with the low frequency resistance of the 1084 sample. In this case a dielectric loss is observed with a retardation time given by the product of 1085 the polarization capacitance and sample resistance. Electrode polarization effects in solid 1086 electrolytes can often be a serious problem and are discussed in §2.3.6.1 and §2.3.6.4 below.

1087 In terms of the equivalent circuit the components of the complex permittivity are (see
 1088 Appendix 2.3)
 1089

1090 
$$\varepsilon'(\omega) = \frac{\sigma''}{e_0 \omega} = \left(\frac{1}{C_0}\right) \left(C_p + \frac{C_s}{1 + \omega^2 \tau_E^2}\right)$$
(2.153)

1091

1092 and 1093

1094  $\varepsilon''(\omega) = \frac{\sigma'}{e_0 \omega} = \left(\frac{C_s}{C_0}\right) \left(\frac{\omega \tau_E}{1 + \omega^2 \tau_E^2}\right) + \frac{\sigma_0}{e_0 \omega}.$ (2.154)
1095

1096 that reproduce the Debye relations eqs. (2.127) and (2.128). The low and high frequency limits 1097 of  $\varepsilon'$  are

1099 
$$\lim_{\omega \to 0} \varepsilon'(\omega) = \varepsilon_0 = \left(\frac{C_p + C_s}{C_0}\right)$$
(2.155)

1100

1098

- 1101 and
- 1102

1103 
$$\lim_{\omega \to \infty} \varepsilon'(\omega) = \varepsilon_{\infty} = \left(\frac{C_p}{C_0}\right).$$
(2.156)

#### Page 34 of 61

1105 Matlab®/GNUOctave codes for computing  $M^*(i\omega)$  and  $\rho^*(i\omega)$  with the added  $R_p$  are given in 1106 Appendix 2.2. A notable result is that  $M^*(i\omega)$  exhibits two relaxations corresponding to the 1107 Debye relaxation and an additional relaxation due to  $\sigma_0$ . The Debye relaxation for  $M^*(i\omega)$  is 1108 unaffected by  $R_p$  but the conductivity relaxation due to  $\sigma_0$  is.

1109 The occurrence of a dielectric and conductivity relaxation together raises an important nomenclature issue that has produced much confusion: the subscripts for denoting limiting low 1110 and high frequency limits can be ambiguous because these limits can refer to either the average 1111 1112 dielectric relaxation frequency or to the average conductivity relaxation frequency. In particular, the quantity  $\varepsilon_{\infty}$  that enters into the expression for the conductivity relaxation time, 1113  $\langle \tau_D \rangle = e_0 \varepsilon_{\infty} / \sigma_0$ , is the high frequency limit for the conductivity relaxation, that may correspond 1114 to the low frequency limit for a separate dielectric relaxation. A proposed nomenclature to 1115 resolve this ambiguity was given above in §2.1. 1116

1117 The "absolute" high frequency limits  $\omega \to \infty$  and  $\omega \to 0$ , rather than 1118  $\{\omega \tau_E, \omega \tau\} \to \infty, 0$  are

1119

1120 
$$\lim_{\omega \to 0} M' = \frac{\varepsilon_{\infty}^{E} \omega^{2} \tau_{E}^{2}}{\left(\varepsilon_{\infty}^{E}\right)^{2} \omega^{2} \tau_{E}^{2}} \to \frac{1}{\varepsilon_{\infty}^{E}}$$
(independent of  $\sigma_{0}$ ) (2.157)

- 1121
- 1122 and
- 1123

1124 
$$\lim_{\omega \to \infty} M'' = \frac{\omega \tau_E \left(\varepsilon_0^E - \varepsilon_\infty^E\right) + \sigma_0 \tau_E / e_0}{\left(\varepsilon_\infty^E\right)^2 \omega^2 \tau_E^2} \to 0 \quad \text{(independent of } \sigma_0\text{)}$$
(2.158)

1125

1126 2.3.5 Interfacial Polarization

In a homogeneous material  $\vec{\nabla} \cdot \vec{\mathbf{D}} = \mathbf{e}_0 \varepsilon \vec{\nabla} \cdot \vec{\mathbf{E}} = 0$  implies  $\vec{\nabla} \cdot \vec{\mathbf{E}} = 0$ . At the interface between 1127 1128 two dielectric materials of different permittivity, however, there is a discontinuity in  $\varepsilon$  and 1129  $\vec{\nabla} \cdot \vec{\mathbf{D}} = 0$  no longer implies  $\vec{\nabla} \cdot \vec{\mathbf{E}} = 0$ . The solution to this problem is obtained by applying Gauss's and Stokes' theorems to the interface with the result that the tangential component of  $\vec{E}$ 1130 1131 is continuous across the interface and the normal component of  $\vec{D}$  is either continuous (no 1132 interfacial charge) or discontinuous if there is a free charge (not the result of polarization of the 1133 materials on each side of the interface). These boundary conditions make interfacial effects 1134 dependent on the geometry of the interface.

1135 Relaxation of interfacial polarization between alternating slabs of insulating dielectric 1136 and conducting layers, generically referred to as a *Maxwell Layered Dielectric*, is characterized 1137 by a single relaxation time  $\tau_i$  given by

Page 35 of 61

1139 
$$\tau_i = R_s C_s = \left(\frac{\ell_R}{\ell_C}\right) \mathbf{e}_0 \rho \varepsilon = \left(\frac{\ell_R}{\ell_C}\right) \left(\frac{\mathbf{e}_0 \varepsilon}{\sigma}\right)$$
(2.159)

1140

1143

where  $\ell_R$  is the thickness of the resistive layer with material resistivity  $\rho$  and  $\ell_c$  is the 1141 thickness of the capacitive layer with material permittivity  $\varepsilon$ . 1142

1144 2.3.6 Maxwell-Wagner Polarization

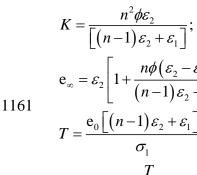
1145 Relaxation of interfacial polarization between a conducting sphere embedded in a 1146 dielectric continuum is known as Maxwell-Wagner (MW) polarization. Wagner [34] computed the observed loss tangent  $(\tan \delta)$  for a volume fraction  $\phi$  of spheres of material conductivity  $\sigma_1$ 1147 and relative permittivity  $\varepsilon_1$  suspended in a dielectric medium of relative permittivity  $\varepsilon_2$ , that was 1148 1149 then generalized by Sillars [35] to suspensions of nonspherical particles. An excellent discussion 1150 of the phenomenon is given in ref [3] from which much of the following is distilled. We also 1151 draw from the paper by van Beek [36] who gave the Sillars formula and then considered the 1152 special case of suspended spheres, and noted that the often cited Wagner formula is only correct 1153 when the permittivities of the suspended material and the dielectric medium are equal and that 1154 the Sillars expression does not have this flaw. 1155

1156

1157 
$$\tan \delta = \frac{\varepsilon_2 K}{\left[ e_{\infty} \left( \varepsilon_2 K + e_{\infty} \right) \right]^{1/2}} \left( \frac{\omega \tau_0}{1 + \omega^2 \tau_0^2} \right)$$
(2.160)

- 1158
- 1159 with

1160



 $\mathbf{e}_{\infty} = \varepsilon_2 \left[ 1 + \frac{n\phi(\varepsilon_2 - \varepsilon_1)}{(n-1)\varepsilon_2 + \varepsilon_1} \right];$  $T = \frac{\mathsf{e}_0\left[\left(n-1\right)\varepsilon_2 + \varepsilon_1\right]}{\sigma_1};$  $\tau_0 = \frac{T}{\left\{ \left( \varepsilon \cdot K + e^{-1} \right) / e^{-1} \right\}^{1/2}},$ 

(2.161)

1162

1163 where a is parallel to the field direction and n is a function of the aspect ratio a/b of the suspended particles. The limiting values for n are 1164 1165

$$n \sim 1 \qquad \qquad \left(a < b\right) \qquad \qquad (a)$$

1166 
$$n=3$$
  $(a=b)$   $(b)$ 

$$n \approx \left\{ \frac{a^2}{b^2 \left[ \ln \left( 2a/b \right) - 1 \right]} \right\} \qquad (a > b) \tag{c}$$

1167

1168 Equation (2.162)(c) indicates that for needle-like particles oriented in the direction of the field 1169 the value of *n* can be large – for example  $n \sim 50$  for a = 10b. Because  $\tan \delta$  is roughly 1170 proportional to  $n^2$  [eqs. (2.160) and (2.161)] the Maxwell-Wagner-Sillars effect can produce very 1171 large dielectric losses. For spherical particles

(2.162)

1172

$$K = \frac{9\phi\varepsilon_2}{\left[2\varepsilon_2 + \varepsilon_1\right]};$$
1173 
$$e_{\infty} = \varepsilon_2 \left[1 + \frac{3\phi(\varepsilon_2 - \varepsilon_1)}{2\varepsilon_2 + \varepsilon_1}\right];$$

$$T = \frac{e_0 \left[2\varepsilon_2 + \varepsilon_1\right]}{\sigma_1},$$
(2.163)

1174

1175 and  $\tau_0$  is unchanged. The maximum value of  $\tan \delta$  is therefore

1176

1177 
$$\tan \delta_{\max} = \frac{\varepsilon_2 K}{2 \left[ e_{\infty} \left( \varepsilon_2 K + e_{\infty} \right) \right]^{1/2}}.$$
 (2.164)

1178

- 1179 This expression is inconveniently complicated but simplifies when  $\phi \rightarrow 0$ :
- 1180

1181 
$$\lim_{\phi \to 0} (\tan \delta_{\max}) = \frac{9\phi\varepsilon_2}{2(2\varepsilon_2 + \varepsilon_1)}$$
(2.165)

1182

1183 The components of the complex relative permittivity for the Maxwell-Wagner phenomenon 1184  $(\phi \rightarrow 0)$  are conveniently expressed using three ancillary functions [36]:

#### 1185

1186 
$$\varepsilon_{\phi} = \varepsilon_2 \left\{ 1 + \frac{3\phi(\varepsilon_1 - \varepsilon_2)}{2\varepsilon_2 + \varepsilon_1} \right\}$$
(2.166)

1188 
$$S = \frac{9\phi\varepsilon_2}{2\varepsilon_2 + \varepsilon_1}$$
(2.167)

168)

1189

1190 
$$T = \frac{\sigma_1}{e_0 \left(2\varepsilon_2 + \varepsilon_1\right)}.$$
 (2.

1191

1192 Then 1193

1194  $\varepsilon'' = \frac{\left(\varepsilon_{\phi} S \omega T\right)}{1 + \omega^2 T^2}$ (2.169)

1195

1196 and 1197

1198 
$$\varepsilon' = \varepsilon_{\phi} \left\{ 1 + \frac{S}{1 + \omega^2 T^2} \right\}.$$
(2.170)

1199

1200 The maximum in the observed dielectric loss  $\varepsilon_{MW}$  is therefore

1201

1202 
$$\varepsilon_{\max}^{"} = \frac{9\phi\varepsilon_{2}^{2}}{2(2\varepsilon_{2}+\varepsilon_{1})} \left[1 + \frac{3\phi(\varepsilon_{2}-\varepsilon_{1})}{2\varepsilon_{12}+\varepsilon_{1}}\right] \rightarrow \frac{9\phi\varepsilon_{2}^{2}}{2(2\varepsilon_{2}+\varepsilon_{1})}$$
(2.171)

1203

1204 that occurs at an angular frequency  $\omega_{max}$  given by

1205

1206 
$$\omega_{\max} = 1/\tau_{MW} = \frac{\sigma_1}{e_0 \left(2\varepsilon_1 + \varepsilon_2\right)}.$$
 (2.172)

1207

1208 At  $\omega_{\max}$  the value of  $\varepsilon'$  from eq. (2.170) is  $\lim_{\phi \to 0} \varepsilon' = \varepsilon_2$  that when combined with eq. (2.171)

1209 produces eq. (2.165).

1210

1211 2.3.7 Examples

1212 Attention is restricted to the dielectric relaxation of water. Emphasis is given to those 1213 techniques that extract information that cannot easily be obtained using the usual formalisms.

- 1214
- 1215 2.3.7.1 Liquid Water

Water is one of the few liquids that relaxes with a single retardation time (or very close to it) and therefore has a Debye complex permittivity. Its dielectric relaxation frequency depends on temperature but always lies within the microwave region of the *em* spectrum. This has important implications for both navigational and meteorological radar and is of course the basis for microwave cooking. The temperature dependence of the retardation time is not Arrhenius but rather adheres to the empirical Fulcher equation (1.543)

1223 
$$\tau = \tau_0 \exp\left(\frac{B}{T - T_0}\right)$$
(2.173)

1224

with parameters  $\tau_0 = 1.25 \times 10^{-13}$  s, B = 669 K,  $T_0 = 138$  K that accurately describes  $\tau(T)$  down to the limit of supercooling of water, ca.  $-35^{\circ}$  C. The relaxation frequency  $(1/2\pi\tau)$  therefore varies between 62 GHz at 0° C and 74 GHz at 100 °C and the energy absorption at 100 °C is about 75% that at 0 °C. Microwave ovens generally operate at a frequency 2.45 GHz that lies on the low frequency side of the Debye dielectric loss peak - the dielectric losses at these temperature extremes are about 4.0% and 3.3% of the maximum loss at  $(1/2\pi\tau)$  Hz.

1231

1232 2.3.7.2 Supercooled Water

Maxwell-Wagner polarization has been used to obtain the relative permittivity of 1233 1234 supercooled water down to about -35°C [37, 38]. The Maxwell-Wagner losses occur in the frequency range  $10^5 - 10^6$  Hz that is far below the frequency range for the dielectric relaxation of 1235 water (around 10<sup>10</sup> Hz). Thus the measured values for the relative permittivity of water 1236 correspond to the limiting low frequency values  $\varepsilon_0 > 80$ . This range is also far above the 1237 relaxation frequency for ice that is about 10<sup>3.5</sup> Hz at 0°C and decreases with decreasing 1238 temperature, so that if crystallization occurred the relevant relative permittivity of ice is the 1239 1240 limiting high frequency value  $\varepsilon_{\infty} \sim 5$ . It is fortunate that the Maxwell-Wagner losses occur at 1241 frequencies between the relaxation frequency ranges of water and ice.

1242 Emulsions of water in heptane stabilized by the surfactant sorbitol tristearate [37] and 1243 droplets suspended in beeswax [38] both exhibit Maxwell-Wagner polarization. In the first and 1244 rigorous beeswax study by Hasted and Shahidi [38] volume fractions of 0.5% and 1.0% were used. Hodge and Angell [37] later used a much larger volume fraction of water (30%) that was 1245 1246 necessitated by their much lower instrumental sensitivity. Their data were stated to be inconsistent with the Maxwell-Wagner formulae because their values of  $\varepsilon'_{max}$  were claimed to 1247 be about four times larger than predicted and their sign of  $(d\varepsilon''_{max}/dT) \propto (d\varepsilon_1/dT)$  was positive 1248 rather than negative as predicted by their eq. (3). However their eq. (3) is incorrect - the 1249 numerator term  $\varepsilon_2^2$  of eq. (2.171) was given as  $\varepsilon_1^2$  so that the analyses of  $\varepsilon_{MW}^*$  given in [1] and 1250 [37] are both incorrect. Equation (2.171) predicts that  $\varepsilon''_{max}$  is indeed inversely proportional to 1251  $\varepsilon_1$  if  $\varepsilon_1 \gg \varepsilon_2$  (a good approximation for water droplets in hexane). The analyses in terms of the 1252 electric modulus [1,37] are unaffected and remain valid although the stated requirement that a 1253 series capacitance that simulates the surfactant layer around the droplet needs to be large for the 1254 1255 modulus analysis to be useful [1] is not correct (see eq. (2.107) above).

1256 The observed maxima in  $\varepsilon''$  decreased with decreasing temperature that is consistent 1257 with eq. (2.171), but for  $\varepsilon_1 \approx 100 \gg \varepsilon_2 \approx 2$  and  $\phi = 0.3$  the predicted value is about 1258  $\varepsilon_{\max}'' \approx \{(9)(0.3)(4)/[2(106)]\} \approx 0.005$ , compared with the experimental values that range 1259 between about 0.4 – 0.8. The predicted value is therefore too large by a factor of about 100. 1260 Also, the measured ratio of  $\varepsilon''_{\max}$  at the temperature extremes of 0°C and -35°C is about 1.8 1261 compared with the correct value of about 1.2. The observed values of  $\omega_{\text{max}}$  for  $\varepsilon$ " were centered 1262 around  $2\pi (5.5 \times 10^6 \text{ Hz}) \approx 3.5 \times 10^7 \text{ rad/s}$  from which eq. (2.172) predicts a conductivity of about

1263 
$$\sigma_1 \approx e_0 \left[ (2\varepsilon_1 + \varepsilon_2) + \phi(\varepsilon_1 - \varepsilon_2) \right] \omega_{\text{max}} / (1 - \phi) \approx (9 \times 10^{-12} \text{ F/m}) (230) (3.5 \times 10^7) / 0.7$$

1264  $\approx (9 \times 10^{-12} \text{ F/m})(230)(3.5 \times 10^7)/0.7 \approx 0.1 \text{ S/m}$  that is impossibly high. Thus the observed  $\varepsilon''$ 1265 data greatly differ from the Maxwell-Wagner predictions.

1266 The measured modulus peak heights also decreased with decreasing temperature and since  $M_{max}$  is assumed to be inversely proportional to the permittivity this trend is also in the 1267 correct direction. Values of  $\varepsilon_1$  for water were then derived by assuming that  $M''_{\text{max}} \propto 1/\varepsilon_1$ , 1268 fixing the proportionality constant from literature data for  $\varepsilon_1$  at 0 <sup>0</sup>C and then least squares fitting 1269 a quadratic in temperature to eight data points between  $0^{\circ}$ C and  $-35^{\circ}$ C. Agreement with the 1270 earlier results, of which the authors were unaware at the time of paper submission (see Note 1271 added in Proof in [37]), was within the  $\pm 2\%$  uncertainties claimed for each method but the 1272 agreement is better than this because most of the discrepancies are systematic due to the different 1273 values of  $\varepsilon_1$  at 0°C for the two methods (measured in [38] but chosen from the literature as a 1274 1275 proportionality constant in [37]). When this is corrected for by equating the average of the 1276 modulus derived permittivities to the average from reference [38] the differences are reduced to 1277 0.5% or less (column four in Table 1). This is a remarkable result given the simplifications used 1278 in the modulus analysis.

1279 These results can be rationalized in terms of a simplified equivalent circuit for the 1280 emulsified water droplets: a parallel ( $R_1C_1$ ) element corresponding to the water droplet with 1281 relative permittivity  $\varepsilon_1$  and conductivity  $\sigma_1$  in series with a capacitance  $C_s$  simulating the 1282 suspected thin layer of interfacial material, and a capacitance  $C_2$  in parallel with the series 1283 combination corresponding to the surrounding heptane. Intuitively,  $C_2$  is much smaller than  $C_1$ 1284 from both geometrical and physical considerations ( $\varepsilon_1 \gg \varepsilon_2$ ). The circuit analysis is:

1285 (i) Admittance  $A_1$  of parallel ( $R_1C_1$ ) element:

1286 
$$A_{1} = 1/R_{1} + i\omega C_{1} = (1 + i\omega R_{1}C_{1})/R_{1} = (1 + i\omega \tau_{1})/R_{1} \text{ so that } Z_{1} = R_{1}/(1 + i\omega \tau_{1}).$$

1287 (ii) Impedance of 
$$\{(R_1C_1)+C_s\}$$
 arm =  $Z_{1s} = \frac{R_1}{1+i\omega\tau_1} + \frac{1}{i\omega C_s} = \frac{i\omega R_1C_s + 1 + i\omega\tau_1}{i\omega C_s(1+i\omega\tau_1)}$ 

$$\Rightarrow A_{1s} = \frac{i \,\omega C_s \left(1 + i \,\omega \,\tau_1\right)}{1 + i \,\omega \left(\tau_1 + R_1 C_s\right)}.$$

1289 (iii) Admittance  $A_{1s2}$  of complete circuit:

1290 
$$A_{1s2} = A_{1s} + i \,\omega C_2 = \frac{i \,\omega C_s - \omega^2 C_s \tau_1 + i \,\omega C_2 \left[1 + i \,\omega \left(\tau_1 + R_1 C_s\right)\right]}{1 + i \,\omega \left(\tau_1 + R_1 C_s\right)}$$

1291 
$$= \frac{i\omega(C_s + C_2) - \omega^2(C_s\tau_1 + C_2\tau_1 - R_1C_sC_2)}{1 + i\omega(\tau_1 + R_1C_s)}$$

1292 (iv) For  $C_2 \ll C_1$  appropriate for water droplets in heptane the admittance simplifies to

Page 40 of 61

1293 
$$A_{1s2} = \frac{i \,\omega C_s - \omega^2 R_1 C_1 C_s}{1 + i \,\omega R_1 \left( C_1 + C_s \right)}$$

1294 Thus

1295

$$C_{1s2}^{*} = \frac{A_{1s2}}{i\omega} = \frac{C_{s}(1+i\omega R_{1}C_{1})}{1+i\omega R_{1}C_{s}} = \frac{C_{s}(1+i\omega R_{1}C_{1})(1+i\omega R_{1}C_{s})}{1+\omega^{2}R_{1}^{2}C_{s}^{2}}$$
$$= \frac{C_{s}-\omega^{2}R_{1}^{2}C_{1}C_{s}}{1+\omega^{2}R_{1}^{2}C_{s}^{2}} + \frac{i\omega C_{s}R_{1}(C_{1}+C_{s})}{1+\omega^{2}R_{1}^{2}C_{s}^{2}}$$
(2.174)

1296 The maximum value of C" is  $(C_1 + C_s)/2$  that is determined in part by the surfactant layer and is 1297 greater than the value  $C_1/2$  for no series capacitance. This is consistent with the observed 1298 maxima in  $\varepsilon$ " [37] being about 100 times greater than that calculated from the Maxwell-Wagner 1299 expression. The maximum in C" also occurs at  $\omega_{max} = 1/(R_1C_s)$  that is determined in part by the 1300 surfactant layer. The dependency of the relaxation time on  $C_s$  can account for the (unreported) 1301 fact that changing the suspending medium changed  $\omega_{max}$  [37] since the suspending medium 1302 would be expected to affect the surfactant layer and  $C_s$ .

1303

The imaginary component of the electric modulus for  $C_2 \ll C_1$  is

1304 
$$M'' = \frac{i \,\omega R_{\rm l}}{\left(1 + i \omega^2 R_{\rm l}^2 C_{\rm l}^2\right)} = \left(\frac{1}{C_{\rm l}}\right) \frac{i \,\omega R_{\rm l} C_{\rm l}}{\left(1 + i \omega^2 R_{\rm l}^2 C_{\rm l}^2\right)},\tag{2.175}$$

1305 the maximum value of which is  $1/(2C_1)$  and therefore contains the desired information about  $C_1$ 1306 that is independent of  $C_s$ . The frequency of maximum M'' is  $\omega_{max} = 1/(R_1C_1)$  and is also 1307 independent of  $C_s$ . Observe that these simplifications arise solely from making  $C_2$  much smaller 1308 than  $C_1$  and do not depend on  $C_s$  being much larger than  $C_1$  as stated earlier [1].

Matlab® and GNUOctave calculations of the relaxation functions for the circuit enable 1309 1310 values of the circuit elements to be quickly estimated that produce trends that are generally consistent with the experimental data, with the notable exception of the maximum values of  $\varepsilon$ " 1311 (discussed briefly below). For example good agreement with the experimental trends is attained 1312 with  $R_1 = 10^3$ ;  $C_1 = 10^{-3}$ ;  $C_2 = 10^{-5}$ ;  $C_s = 5 \times 10^{-4}$ . The value of 100 for the ratio  $C_1/C_2$  was 1313 chosen to approximate the ratio of permittivities of water and hexane and to accommodate an 1314 1315 unknown geometric factor for the suspending medium relative to the droplet, and the value of  $C_s$ was found from the experimental ratio of 0.5 for the frequencies of maximum  $\varepsilon$ " and M" (the 1316 latter being higher). The geometric factor is probably the largest source of uncertainty in the 1317 1318 values of the circuit parameters.

1319 Equation (2.174) indicates that the maximum value of  $\varepsilon$ " should be increased by a factor 1320 of  $(C_1 + C_s)/C_1 \approx 100$  over that for no surfactant, consistent with experiment [37].

1321 The Maxwell-Wagner equivalent circuit discussed here is obviously crude but serves to 1322 rationalize the remarkable success of the electric modulus in analyzing the Maxwell-Wagner 1323 effect for water droplets in a dielectric medium of low permittivity.

1325 2.3.7.3 Hydration Water

Water of ionic hydration is readily probed by dielectric relaxation, if the ionic 1326 conductivity contribution to  $\varepsilon''$  and tan  $\delta$  is sufficiently small. Data for glasses of Ca(NO<sub>3</sub>), 1327 hydrates [39] provide a convenient illustration of how water in different environments can be 1328 1329 distinguished dielectrically. Spectra of dielectric tan  $\delta$  vs. 1/T at 1 Hz were shown for eight glasses of composition  $Ca(NO_3)_2 RH_2O Ca(NO_3)_2 RH_2O (R = 3, 4, 5, 6, 8, 10, 12, 14).$ 1330 Glasses with lower R values required the addition of  $KNO_3$  to ensure glass formation but this 1331 was expected to have only a minor effect on water dynamics because of the larger ionic 1332 charge/radius of K<sup>+</sup> compared with Ca<sup>2+</sup>. Four relaxations were observed: 1333

- 1334  $(\alpha)$  A conductivity relaxation at low 1/T corresponding to the glass transition manifested as 1335 the steep increase in tan  $\delta$ . The relaxation temperature corresponds to tan  $\delta = 1$  (*vide infra*) and 1336 will be referred to as the "conductivity wing". It is essential that this relaxation occur at 1337 sufficiently high *T* in order that the other relaxations occur in the poorly conducting glassy state 1338 and not be hidden beneath the conductivity contribution to tan  $\delta$ .
- 1339  $(\beta)$  A dielectric relaxation lying close to the conductivity wing whose shift in position with *R* 1340 paralleled that of the conductivity relaxation. It was observable only as a shoulder for R=1-61341 and (probably) R=10 but is seen as a clear peak for  $R \approx$  trace.
- 1342  $(\gamma)$  A weak low temperature dielectric relaxation  $(\tan \delta_{\max} \approx 10^{-3} 10^{-2})$  in the 1343  $Ca(NO_3)_2.RH_2O$  system occurred as a broad maximum for R = 4, 5, 6 and as a shoulder for 1344  $R \ge 8$ .
- 1345 ( $\delta$ ) A dielectric relaxation whose intensity increased rapidly with *R*. It is probably a part of 1346 the broad maximum near 10<sup>3</sup>/*T* ≈ 7.5 for *R* = 8 but appeared as a clear maximum for *R* ≥ 10.
- 1347 The  $\beta$  relaxation was assigned to cation bound water that presumably coordinates Ca<sup>+</sup> rather than  $K^+$  because of the larger ionic charge/radius ratio of the former. The rapid shift in 1348 relaxation temperature with R > 1 was interpreted as a change in water dynamics as H<sub>2</sub>O replaces 1349  $NO_3^-$  in the first coordination shell of  $Ca^+$ . The R - invariance for R = trace and R = 1 was 1350 attributed to a single water molecule lying in the first coordination shell. This assignment of the 1351  $\beta$  relaxation to Ca<sup>2+</sup> bound water implied a dielectric activity that merits discussion. The most 1352 plausible geometry for H<sub>2</sub>O coordinated to Ca<sup>+</sup> is when the H<sub>2</sub>O dipole points away from the 1353 Ca+ ion. However if this held in the complex ionic environment of the glass there would be no 1354 dielectric activity because the rotational axis would bisect the H-O-H angle and coincide with 1355 1356 the dipole vector. Two alternatives suggest themselves:
- 1357 (1) Exchange of water and nitrate in the coordination shell. This implies an associated 1358 volume fluctuation and ultrasonic activity. Such activity has been observed [40,41] in 1359  $Ca(NO_3)_2 \cdot RH_2O$  solutions at about 20 MHz at room temperature. This relaxation moved to 1360 higher frequencies with increasing *R* and the edge of a second relaxation at higher frequencies 1361 was noted, both being consistent with the glassy state dielectric behavior. Such an exchange 1362 would also be expected to contribute to the translational ionic migration that produces 1363 conductivity, consistent with the essentially *R* – invariant difference between the  $\alpha$  and  $\beta$

#### Page 42 of 61

relaxation temperatures. The possibility that this relaxation is part of a conductivity relaxation with a distribution of relaxation times is discussed in §2.5.

1366 A different  $Ca^+$ -OH<sub>2</sub> geometry is favored in which the dipole vector and rotation axis do (2)not coincide. Neutron diffraction data indicate this occurs in CaCl<sub>2</sub> and NiCl<sub>2</sub> solutions [42], in 1367 which an angle of ca. 40° was observed between the dipole and coordination axes at R = 12.61368 (NiCl<sub>2</sub>) and 12.3 (CaCl<sub>2</sub>), and about 0° in dilute solutions ( $R \approx 450$ ). It was not possible to 1369 find the dielectric activity per water molecule of the  $\beta$  relaxation in the Ca(NO<sub>3</sub>)<sub>2</sub>·RH<sub>2</sub>O 1370 glasses because of overlap with the conductivity wing and the  $\gamma$  relaxation, but for the mixed 1371 1372 nitrate glasses the well-defined conductivity wing for the anhydrous mixture could be shifted and 1373 subtracted to yield plausibly shaped peaks of  $\tan \delta$  vs. 1/T. The peak heights and widths in the R = 1 and R = 3 glasses were about the same so that barring an unlikely ratio of activation 1374 energies in excess of 3 it appears that the dielectric activity per water molecule does indeed 1375 decrease with increasing R. A crude calculation indicated that the observed values of  $\tan \delta_{\max}$ 1376 yielded sensible values of  $\Delta \theta$ . The dipole being relaxed was assumed to be the component of 1377 the water dipole  $(\mu_w)$  orthogonal to the rotation axis, magnitude  $\mu_w \sin(\Delta\theta)$ , and  $\tan \delta_{\max}$  was 1378 assumed to be proportional to  $(\varepsilon_0 - \varepsilon_{\infty})$  that is in turn proportional to  $R \left[ \mu_W \sin(\Delta \theta) \right]^2$ . Equating 1379

1380  $\tan \delta_{\max}$  for the 1*R* and 3*R* glasses then yielded

1381 
$$\frac{3}{T_{3R}}\sin^2(\Delta\theta_{3R}) = \frac{1}{T_{1R}}\sin^2(\Delta\theta_{1R}),$$
 (2.176)

1382 so that

1383 
$$\sin^2(\Delta\theta_{3R}) \approx 0.286 \sin^2(\Delta\theta_{1R}).$$
 (2.177)

Examples of  $\{\Delta \theta_{1R}, \Delta \theta_{3R}\}$  pairs were  $\{60^{\circ}, 28^{\circ}\}$  and  $\{30^{\circ}, 15^{\circ}\}$ , both of which were sensible values and roughly comparable with the neutron diffraction values.

For large values of *R* the  $\delta$  relaxation was expected to resemble pure water so that an extrapolation to infinite dilution should yield the temperature at which the relaxation frequency of water is 1 Hz. The retardation temperatures at 1 Hz for the  $\delta$  relaxation in four aqueous glasses (solutions of Ca(NO<sub>3</sub>)<sub>2</sub>, CaZnCl<sub>4</sub>, Li<sub>2</sub>ZnCl<sub>4</sub> and ZnCl<sub>2</sub>) all extrapolated to about 162±5 K at infinite dilution, strongly suggesting that the relaxation temperature for pure water would be 162±5 K at 1Hz. The temperature dependence of the relaxation time for water between -20°C to +30°C [43] was found to follow the Fulcher equation

1393 
$$\tau(T) = \tau_0 \exp\left(\frac{B}{T - T_0}\right)$$
(2.178)

with  $A = 1.25 \times 10^{-13}$  s, B = 669 K,  $T_0 = 138$  K. The extrapolated {1 Hz,  $162 \pm 5$  K} datum agreed with the Fulcher value {1 Hz, 162 K} (uncertainties not stated). Given the large extrapolation over about 11 orders of magnitude this agreement constitutes strong evidence that dielectric relaxation of water outside the first coordination shell of the Ca<sup>2+</sup> and Li<sup>+</sup> cations is the same as pure water. A similar extrapolation of LiCl in glycerol data yields a relaxation temperature equal to the directly observable value for pure glycerol at 1 Hz. 1401 2.4 Conductivity Relaxation

1402 2.4.1 General Aspects

1400

1403 As noted earlier relaxation of polarization can occur either by translation of electric 1404 charge (electric current) or by dipole rotation (displacement current). Thus polarization induced 1405 by an electric field can occur by *conductivity relaxation* [44] arising from long range 1406 translational migration of point charges as well as by the dielectric relaxation considered so far 1407 (dipole rotation or localized hopping of ions between sites). The time scale associated with a 1408 frequency invariant conductivity  $\sigma_0$  defined by

1409 
$$\langle \tau_D \rangle = \sigma_0 / e_0 \varepsilon_{\infty}$$
 (2.179)

1410 (see eq. 1.42 Chapter One), but this time scale is not evident in  $\sigma'$  vs ln  $\omega$  plots nor is it for the 1411 monotonic function  $\varepsilon^* = \varepsilon' - i\sigma_0 / e_0 \omega$ . However  $\rho''$  and M'' clearly indicate the time scale 1412 because they exhibit maxima in the frequency domain at  $\omega \approx 1/\langle \tau_D \rangle$ . The time constant  $\tau_D$  in 1413 eq. (2.179) differs from the characteristic time  $\tau_e$  in the Fermi gas expression for electronic 1414 conductivity in metals, which is directly proportional to  $\sigma_0$  [45]:

1415 
$$au_e = \frac{m}{ne^2}\sigma_0,$$
 (2.180)

1416 where *n* is the number density of charge carriers of effective mass *m* and charge *e*. The reason for the difference is that  $\tau_e$  is the average time of travel between scattering events (collisions with 1417 ions, electrons or phonons or by umklapp), whereas  $\tau_D$  is the residence time between 1418 (effectively instantaneous) jumps between adjacent sites. Nor is  $\tau_{\scriptscriptstyle D}$  equal to  $\tau_{\scriptscriptstyle E}$  for dielectric 1419 1420 relaxation, although they are related by an expression to be derived later. As noted already the relaxation time  $\tau_D$  is a measure of the rate of decay of the polarization at constant displacement, 1421 i.e. the decay of the electric field E at constant D [44], whereas the dielectric retardation time is a 1422 1423 measure of the decay rate of the polarization at constant E, i.e. of D at constant E.

Equation (2.179) implies that ionic conductivity cannot exceed ca.  $10^3$  Sm<sup>-1</sup>, since  $\tau_D$ cannot reasonably be less than a vibrational lifetime and  $\varepsilon_{\infty}$  is rarely greater than about 10. The vibrational  $\tau_v$  lifetime is conveniently defined by the condition for critical damping (§1.11),  $\omega_0 \tau_v = 1$ , so that for a typical vibrational frequency of about  $f \approx 10^{12}$  Hz  $\Rightarrow \omega \approx 6 \times 10^{12}$  rad/s the value of  $\tau_v$  is about  $2 \times 10^{-13}$  s and

1429 
$$\sigma_{0,\max} \approx \frac{e_0 \varepsilon_{\infty}}{\tau_V} \approx \frac{\left(8.854 \times 10^{-12} \text{ F/m}\right)(10)}{2 \times 10^{-13} \text{ s}} \approx 400 \text{ S/m}$$
 (2.181)

1430 that is comparable with the highest conductivity observed for ionic conductors.

1431 The properties of the four basic functions for conductivity relaxation are conveniently 1432 illustrated using a circuit comprising three elements in series: (i) a capacitance  $C_s = 10^{-6} \text{ F} = 1\mu\text{F}$ 1433 ; (ii) a parallel combination of a resistance  $R_1 = 10^8 \Omega$  and a capacitance  $C_1 = 10^{-12} \text{ F}(1\text{pF})$  (iii) 1434 another parallel combination of a resistance  $R_2 = 10^6 \Omega$  and a capacitance  $C_1 = 10^{-12} \text{ F}(1\text{pF})$ .

#### Page 44 of 61

The two parallel  $R_p$  -  $C_p$  elements could for example simulate crystal and inter-crystal impedances in a polycrystalline samples and the series capacitance  $C_s$  could simulate electrode polarization. As discussed below this circuit has been used by several groups and will be referred to as the "ideal conductivity" circuit. A Matlab®/GNU Octave code for generating the corresponding spectra for the real and imaginary components of the four basic complex relaxation functions (§2.1.9), and the corresponding complex plane plots of the imaginary component vs. the real component, is given in Appendix AA.

We discuss next the controversial electric modulus function (a discussion of many of the issues surrounding it is given in [1]). The electric modulus  $M^* = M' + iM''$  appears to have been first defined by McCrum, Read and Williams [32], but its use in analyzing conductivity relaxation was first initiated and exploited by Macedo and coworkers [44]. The usefulness of  $M^*$ is illustrated by the simplest case of a constant conductivity  $\sigma_0$  and constant relative permittivity  $\varepsilon_{\infty}$  (the reason for the subscripts will become clear when distribution functions are considered later). For convenience we copy eq. (2.101) here:

$$M' = \frac{\varepsilon'}{\varepsilon'^2 + \varepsilon''^2}$$
(a)  

$$M'' = \frac{\varepsilon''}{\varepsilon'^2 + \varepsilon''^2}$$
(b).

1450 Insertion of the relations  $\varepsilon'' = \sigma_0 / e_0 \omega$  and  $\varepsilon' = \varepsilon_{\infty}$  then yields

1451 
$$M' = \frac{1}{\varepsilon_{\infty}^{D}} \left( \frac{\omega^{2} \tau_{D}^{2}}{1 + \omega^{2} \tau_{D}^{2}} \right)$$
(2.183)

1452 and

1453 
$$M'' = \frac{1}{\varepsilon_{\infty}^{D}} \left( \frac{\omega \tau_{D}}{1 + \omega^{2} \tau_{D}^{2}} \right).$$
1454 (2.184)

1455 Thus M'' exhibits the desired (symmetric) peak as a function of  $\ln(\omega)$ . The components of  $\rho^*$ 1456 are related to those of  $M^*$  by

1457 
$$\rho' = \frac{M''}{e_0 \omega} = \frac{\tau_D}{e_0 \varepsilon_{\infty}^D} \left( \frac{1}{1 + \omega^2 \tau_D^2} \right) = \left( \frac{\rho_0}{1 + \omega^2 \tau_D^2} \right)$$
(2.185)

1458 and

1459 
$$\rho'' = \frac{M'}{e_0 \omega} = \frac{\tau_D}{e_0 \varepsilon_\infty^D} \left( \frac{\omega \tau_D}{1 + \omega^2 \tau_D^2} \right) = \rho_0 \left( \frac{\omega \tau_D}{1 + \omega^2 \tau_D^2} \right), \qquad (2.186)$$

1460 where  $\rho_0 = 1/\sigma_0 = \tau_D / e_0 \varepsilon_{\infty}^D$ . Note that M'' and  $\rho''$  have identical frequency dependencies but 1461 are weighted by  $1/\varepsilon_{\infty}$  and  $\rho_0$  respectively. This difference in weighting factors can be exploited 1462 to considerable advantage in the analysis of ac conductivity (§2.3.5.6-§2.3.5.8).

For dielectric relaxation  $M^*$  and  $\varepsilon^*$  are almost equivalent because a Debye peak in  $\varepsilon''$ also yields a Debye peak in M'' [44] [see eqs. (2.132) and (2.133)]. The derivation for a Debye dielectric without any conductivity is given in Appendix 2.1. It might appear that a peak in M''the due to either a conductivity or dielectric process and that  $M^*$  could not distinguish

- 1467 between them. This is not necessarily so, however, because the average relaxation time  $\langle \tau_D \rangle$  will 1468 be calculable from the limiting low frequency conductivity [eq. (2.73)] if the process is a 1469 conductivity relaxation. If the peak in *M*" is due to dielectric relaxation the retardation time will 1470 not correlate with  $\sigma_0$ . The archetypal example of dielectric relaxation being correlated with  $\sigma_0$ 1471 occurs in the alkali silicate glasses and it was this correlation that originally led to the inference 1472 that the residual dielectric loss (after subtraction of  $\sigma_0 / e_0 \omega$ ) is due to the same alkali migration
- 1473 process that produces  $\sigma_0$  [27-31]. This led Macedo and collaborators [44] to first use  $M^*$  in the
- 1474 analysis of conductivity relaxation.
- 1475 Note also that for dielectric relaxation

1476 
$$\lim_{\omega \to 0} M'_{dielectric}(\omega) = 1/\varepsilon_0$$
(2.187)

1477 compared with  $\lim_{\omega \to 0} M'_{conductivity}(\omega) = 0$  for conductivity relaxation. The low frequency 1478 conductivity relaxation limit for M' is revealing conceptually because M' is a measure of the 1479 restoring force in response to an electric field perturbation. The low frequency limit of this 1480 restoring force is finite for dielectric relaxation because the charge storage ability remains 1481 nonzero:  $\lim_{\omega \to \infty} \varepsilon'(\omega) = \varepsilon_0$ . For conductivity relaxation the dielectric loss becomes infinite as

1482  $\omega \rightarrow 0$  (dissipation completely overrides any storage capability) and the restoring force is "short 1483 circuited". This is precisely analogous to the mechanical modulus going to zero as the viscosity 1484 of a viscoelastic material dominates at low frequency and the elasticity disappears. The electric 1485 modulus was first introduced to emphasize this mechanical analogy [32].

1486 An alternative to the electric modulus for analyzing materials in which the dielectric loss 1487 and conductivity are correlated has been proposed by Johari [46]. This proposal is similar in style 1488 to a mechanism for ionic conductivity proposed by Hodge and Angell [47] that was based on the 1489 one-dimensional Glarum diffusion model for dielectric relaxation [§1.12.6, Chapter One]. Recall 1490 that the Glarum model comprises a relaxing dipole that can relax either independently with retardation time  $\tau_0$  or by the arrival of a defect of some kind that relaxes it instantly. Hodge and 1491 Angell suggested that the dipole is a trapped ion/vacancy pair (that is known to exhibit Debye 1492 dielectric behavior) and that the defects are itinerant ions that contribute to  $\sigma_0$ . The average 1493 1494 activation energy for oscillation of trapped ions and that for ion migration are presumed to be 1495 similar (perhaps identical), thus accounting for the nearly temperature invariant distribution of 1496 conductivity relaxation times. The Glarum function is mathematically similar to the Davidson-1497 Cole function that has a Debye-like low frequency loss that is rarely observed. This low 1498 frequency behavior arises from the Glarum assumption that the dipole has just one retardation 1499 time. However if a distribution of dipole retardation times is assumed, corresponding to a 1500 distribution of sites in an amorphous material for example, better agreement with experiment is 1501 obtained without changing the essential physics of the Glarum model.

1502

1503 2.4.2 Distribution of Conductivity Relaxation Times

1504 Both  $M^*$  and  $\rho^*$  can be described in terms of a distribution of conductivity relaxation 1505 times: Page 46 of 61

1506 
$$M^{*}(i\omega) = M_{\infty} \int_{-\infty}^{+\infty} g\left(\ln\tau_{D}\right) \left(\frac{i\omega\tau_{E}}{1+\omega^{2}\tau_{D}^{2}}\right) d\ln\tau_{D}$$
(2.188)

and similarly for  $\rho^*(i\omega)$ . A distribution of conductivity relaxation times affects the dispersion of the corresponding complex admittance functions  $\varepsilon^*(i\omega)$  and  $\sigma^*(i\omega)$ :

1509 
$$\sigma_0 = \frac{\mathbf{e}_0 \mathcal{E}_{\infty}^D}{\left\langle \tau_D \right\rangle} = \frac{\mathbf{e}_0}{M_{\infty}^D \left\langle \tau_D \right\rangle},\tag{2.189}$$

1510 
$$\sigma_{\infty} = e_0 \varepsilon_{\infty}^D \left\langle \frac{1}{\tau_D} \right\rangle = \frac{e_0}{M_{\infty}^D} \left\langle \frac{1}{\tau_D} \right\rangle , \qquad (2.190)$$

1511 and

1522

1512 
$$\varepsilon_0^D = \varepsilon_\infty^D \frac{\left\langle \tau_D^2 \right\rangle}{\left\langle \tau_D \right\rangle^2} \ge \varepsilon_\infty^D. \tag{2.191}$$

1513 A distribution of conductivity relaxation times is not easily distinguishable from 1514 dielectric and conductivity relaxations occurring together in modulus spectroscopy [36,44] 1515 although the dielectric relaxation will not be observable if  $\tau_E \gg \tau_D$  because  $\sigma_0$  will then exceed 1516 the limiting high frequency dielectric conductivity given by eq. (2.131):

1517 
$$\frac{\sigma'(\omega\tau_D \to 0)}{\sigma'_{\mu}(\omega\tau_E \to \infty)} = \frac{\sigma_0}{\sigma_{\mu}(\infty)} = \frac{\varepsilon_{\infty}}{\langle \tau_D \rangle} \left( \frac{\langle \tau_E \rangle}{\varepsilon_0 - \varepsilon_{\infty}} \right) = \frac{\varepsilon_{\infty}}{\varepsilon_0 - \varepsilon_{\infty}} \frac{\langle \tau_E \rangle}{\langle \tau_D \rangle} >> 1.$$
(2.192)

This phenomenon has been directly observed in systems for which the dielectric retardation time is essentially constant but whose conductivity is increased by addition of electrolyte [48, 49] (see \$2.3.6.9 below). This problem is ameliorated if conductivities can be measured with very high precision [50].

- 1523 2.4.3 Constant Phase Element Analysis
- 1524 It is sometimes useful to have a circuit element for which the phase angle is independent 1525 of  $\omega$ ,

1526 
$$W^*(i\omega) = W(\omega) \exp\left(\pm \frac{i\,\alpha\pi}{2}\right),\tag{2.193}$$

1527 where  $W(\omega)$  is any real function and  $0 < \alpha \le 1$  is real; the positive sign in the exponent 1528 corresponds to an admittance and the negative sign to an impedance. As noted in Chapter One 1529 and §2.4.3, however, eq. (2.193) can only be valid over a restricted frequency range since 1530 otherwise the underlying distribution of relaxation/retardation times cannot be normalized. 1531 Equation (2.193) is a generalization of the Warburg impedance for which  $\alpha = 0.5$ .

1532 Almond and West [51] suggested the addition of such a parallel constant phase element 1533 admittance W [eq (2.193)] to the ideal parallel  $R_pC_p$  element, in order to better simulate the 1534 typical admittance of solid electrolytes. The electrical response functions for this circuit are:

1535 Conductivity

Page 47 of 61

1537 where  $k = \text{geometric cell constant}, W_0' = k W_0 \cos(\alpha \pi / 2), W_0'' = k W_0 \sin(\alpha \pi / 2).$ 1538

1539 *Relative Permittivity* 

1540 
$$\varepsilon_{AW}^{*}(i\omega) = \frac{\sigma^{*}(i\omega)}{i\varepsilon_{0}\omega} = \left\{ \left[ \varepsilon_{\infty} + \left(\frac{W_{0}^{''}}{e_{0}}\right)\omega^{\alpha-1} \right] - i\left[\frac{\sigma_{0}}{e_{0}\omega} + \left(\frac{W_{0}^{'}}{e_{0}}\right)\omega^{\alpha-1} \right] \right\}$$
(2.195)

1541

1542 Electric Modulus

$$M_{AW}^{*}(i\omega) = \frac{i\omega\varepsilon_{0}}{\sigma^{*}(i\omega)} = \frac{i\omega\varepsilon_{0}}{\left[\sigma_{0} + W_{0}^{'}\omega^{\alpha}\right] + i\left[e_{0}\varepsilon_{\infty}\omega + W_{0}^{''}\omega^{\alpha}\right]}$$

$$= \frac{\omega\varepsilon_{0}\left[\left(\varepsilon_{0}\varepsilon_{\infty}\omega + W_{0}^{''}\omega^{\alpha}\right) + i\left(\sigma_{0} + W_{0}^{'}\omega^{\alpha}\right)\right]}{\left[\sigma_{0} + W_{0}^{'}\omega^{\alpha}\right]^{2} + \left[\varepsilon_{0}\varepsilon_{\infty}\omega + W_{0}^{''}\omega^{\alpha}\right]^{2}} \times \left(\frac{\varepsilon_{\infty}/\sigma_{0}^{2}}{\varepsilon_{\infty}/\sigma_{0}^{2}}\right)$$

$$= \left(\frac{1}{\varepsilon_{\infty}}\right)\frac{\omega\tau_{D}\left\{\left[1 + \left(\frac{W_{0}^{''}}{\sigma_{0}}\right)\omega^{\alpha}\right] + i\left[e_{0}\varepsilon_{\infty}\omega + \left(\frac{W_{0}^{'}}{\sigma_{0}}\right)\omega^{\alpha}\right]\right\}}{\left[1 + \left(\frac{W_{0}^{'''}}{\sigma_{0}}\right)\omega^{\alpha}\right]^{2} + \left[e_{0}\varepsilon_{\infty}\omega + \left(\frac{W_{0}^{''}}{\sigma_{0}}\right)\omega^{\alpha}\right]^{2}}$$

$$= 1544 \quad \text{Exerction (2.10) with the other weaklikhed wave d. We step for example, the other value of the second traces are shown in the second trac$$

1544 Equation (2.19) yields the published Almond-West form with the substitutions 1545  $x = \omega \left( W_0^{\prime} / \sigma_0 \right)^{1/\alpha} = \left[ \left( \sigma' - \sigma_0 \right) / \sigma_0 \right]^{1/2} \text{ and } \omega \tau_D = \left[ \left( \sigma_0^{\prime} / W_0^{\prime} \right)^{1/\alpha} \left( e_0 \varepsilon_{\infty} / \sigma_0 \right) \right] x = Qx:$ 

1546 
$$M_{AW}^{*}(i\omega) = \left(\frac{Qx}{\varepsilon_{\infty}}\right) \frac{\left\{\left[Qx + \tan\left(\frac{\alpha\pi}{2}\right)x^{\alpha}\right] + i\left[1 + x^{\alpha}\right]\right\}}{\left[1 + x^{\alpha}\right]^{2} + \left[Qx + \tan\left(\frac{\alpha\pi}{2}\right)x^{\alpha}\right]^{2}}$$
(2.197)

1547

1548 Resistivity

1549 
$$\rho_{AW}^{*}(i\omega) = \frac{1}{\sigma^{*}(i\omega)} = \frac{M^{*}(i\omega)}{i\epsilon_{0}\omega} = \rho_{0} \frac{\left(1 + x^{\alpha}\right) - i\left[Qx + \tan\left(\frac{\alpha}{2}\right)x^{\alpha}\right]}{\left(1 + x^{\alpha}\right)^{2} + \left[Qx + \tan\left(\frac{\alpha}{2}\right)x^{\alpha}\right]^{2}}$$
(2.198)

Page 48 of 61

1550

1551 2.4.4 Determination of  $\sigma_0$ 

1552 Several methods are available for estimating  $\sigma_0$  when electrode polarization and 1553 intergranular impedances obscure the limiting low frequency conductivity plateau. An accurate value for  $\sigma_0$  is important because, in addition to the obvious need for reliable data, its 1554 1555 contribution to  $\varepsilon$ " must be subtracted for permittivity analyses (the attendant difficulties have been discussed by Ravaine and Souquet [52, 53]). Accurate values of  $\sigma_0$  are also needed in 1556 1557 order to determine reliable activation energies for conductivity. For example if  $\log(\sigma)$  measured at constant measuring frequency  $\omega_{meas}$  is plotted against 1/T in the usual Arrhenius fashion, 1558 spurious changes in slope can result from both polarization and bulk relaxation effects. If  $\omega_{meas}$ 1559 lies in a region where polarization is significant then the measured conductivity will be less than 1560 1561  $\sigma_0$  by an amount that increases with increasing temperature, because of the shift to higher frequencies of the polarization  $\sigma'$  spectrum (which has essentially the same effective activation 1562 energy as the sample conductivity). A fictitiously low activation energy is then obtained at high 1563 temperatures as  $\omega_{meas}$  probes deeper into the polarization relaxation. A spuriously low activation 1564 energy can also occur at low temperatures when  $\omega_{meas}$  lies within the bulk relaxation frequency 1565 range, where  $\sigma'$  is often observed to increase as  $\omega^{\alpha}(\alpha < 1)$ . In this case the measured 1566 conductivity will exceed  $\sigma_0$  by an amount that decreases with increasing temperature and the 1567 1568 measured activation energy will be smaller than the true value by the factor  $\alpha = d \ln \sigma' / d \ln \omega$ :

1569 
$$E_{a,obs} = E_{a,true} \left( 1 - \alpha \right).$$

1570 In cases where  $\alpha \approx 1$ , as occurs in some electronic semiconductors [48], the fixed frequency 1571 conductivity is therefore almost independent of temperature in the bulk relaxation temperature 1572 region.

(2.199)

1573

### 1574 2.4.4.1 Analyses in the Complex Resistivity Plane

Ravaine and Souquet [52,53] used the complex resistivity plane for determining  $\sigma_0$  of 1575 1576 alkali silicate glasses in the presence of electrode polarization by low frequency extrapolation to 1577 the real axis. They fitted the high frequency spectrum (i.e. sample relaxation) to the Cole-Cole 1578 [54] function (see §1.12.5) and extrapolated the Cole-Cole semicircle to the real axis. For severe polarization Armstrong et al. [55-59] used a similar method based on extrapolation of the high 1579 1580 frequency polarization spike to the real axis. This method is restricted to high conductivities 1581 whose relaxation frequency lies above the measuring frequency range. As noted earlier the spike 1582 sometimes occurs at an angle to the real axis rather than the ideal right angle that has been 1583 attributed to "surface roughness" at the electrode interface [55].

1584

# 1585 2.4.4.2 Modulus and Resistivity Spectra

1586 In cases where polarization and conductivity relaxations overlap significantly and no 1587 plateau in  $\sigma'$  is observed,  $\sigma_0$  can be estimated from eq. (2.179) if  $\langle \tau_D \rangle$  and  $\varepsilon_{\infty}$  are known. 1588 These can often be determined with sufficient precision by fitting  $M''(\omega)$  to an appropriate 1589 empirical function: only the bulk relaxation is included in the fitted function because of the 1590 insensitivity of *M*" to high capacitance effects such as polarization and intergranular impedances. 1591 For this application the fit to *M*" should be weighted by the lower frequency data because these 1592 reflect the longer relaxation time components of the distribution that contribute more 1593 significantly to  $\langle \tau_D \rangle$ . The maximum in  $\rho$ ",  $\rho_{max}$ , can also be used to estimate  $\sigma_0$ : if the full 1594 width at half height of the peak in  $\rho$ " is  $\Delta$  decades, then  $\sigma_0$  can be estimated to within about 1595  $\pm 10$  % from the empirical relation

1596 
$$\sigma_0 \approx \frac{1}{1.75 \Delta \rho_{\text{max}}}$$
 (2.200)

1597 If only the maximum in  $\rho$ " at  $\omega_{max}$  is observable  $\sigma_0$  can still be estimated from the value of  $\rho'$ 1598 at  $\omega_{max}$  by assuming  $\rho''(\ln \omega)$  to be symmetric:

1599 
$$\sigma_0 \approx \frac{1}{2\rho'(\omega_{\text{max}})}.$$
 (2.201)

1600

1601 2.4.4.3 Complex Admittance Plane

1602 One of the first applications of complex plane plots was to polycrystalline yttria-zirconia electrolytes by Bauerle [60]. Bauerle gave an excellent discussion of equivalent circuits and their 1603 corresponding complex admittance plane plots, but the only circuit used in their data analysis 1604 was a series combination of two parallel  $R_p C_p$  elements and a series resistance  $R_s$ . One of the 1605 parallel  $R_pC_p$  elements in this circuit represents the electrode interface: the capacitance of a 1606 1607 double layer (electrode polarization) in parallel with the resistance of an oxygen gas-oxide ion charge transfer process. The second  $R_pC_p$  element represents an intergranular boundary 1608 1609 ("constriction") impedance, and the pure resistance simulates the bulk crystal. The 1610 experimentally observed complex admittance plane plots were in excellent agreement with the 1611 equivalent circuit behavior. The zero frequency conductivity predicted from the complex plane 1612 plot was also in excellent agreement with four terminal data, and the expected dependence of the 1613 electrode impedance on oxygen partial pressure was observed. Despite these successes, some 1614 disadvantages of the method should be pointed out. First, in assuming that the bulk crystal acts as 1615 a pure resistance the analysis implicitly assumes that the measuring frequencies are well below the conductivity relaxation frequency, that can only be confirmed retrospectively. Second, 1616 1617 although there are three relaxing elements (since the sample resistance must realistically have a 1618 capacitance in parallel with it), the complex admittance plane exhibits only two arcs that reflect 1619 the differences between the relaxing elements. If the observed relaxations overlap significantly, 1620 an assumption must be made about the shapes of the two relaxations before extrapolations are made, i.e. a functional form for the extrapolating function must be chosen. Bauerle's data were 1621 1622 well described by the Cole-Cole function but this would not be expected to occur in general.

1623

1624 2.4.5 Combined Conductivity and Dielectric Relaxation

1625 These two relaxation phenomena can occur together provided the conductivity relaxation 1626 occurs at lower frequencies than any dielectric relaxation, otherwise the increase in  $\varepsilon$ " as *f* 1627 decreases will dominate any dielectric loss.

#### Page 50 of 61

1629 2.4.6 Examples

1630 2.4.6.1 Electrode Polarization and Bulk Relaxation in the Frequency Domain

1631 Consider an idealized equivalent circuit similar to that used by Bauerle in which the series resistance is replaced by a series capacitance. Specific values of the parallel  $R_p C_p$  elements 1632 are  $\left[R_1 = 10^8 \Omega, C_1 = 10^{-11} \mathrm{F} \Longrightarrow \tau_1 = R_1 C_1 = 10^{-3} \mathrm{s}\right], \left[R_2 = 10^6 \Omega, C_2 = 10^{-11} \mathrm{F} \Longrightarrow \tau_2 = R_2 C_2 = 10^5 \mathrm{s}\right]$  and 1633  $\begin{bmatrix} C_s = 10^{-6} \end{bmatrix}$  so that the distribution of conductivity relaxation times comprises two delta 1634 functions at  $\tau_1 = 10^{-3}$  s and  $\tau_2 = 10^{-5}$  s. The shorter relaxation time element simulates the crystal 1635 impedance in a polycrystalline preparation, the longer relaxation time element simulates an 1636 1637 intergranular impedance, and the series capacitance simulates electrode polarization. This circuit has been found to be qualitatively useful in describing the electric response of a variety of 1638 1639 conductors, including a superionic conductor [61], an electronic semiconductor [62], and a normal ionic conductor [9]. The relaxation time averages are 1640

1641 
$$\left\langle \tau_D^2 \right\rangle = \frac{\tau_1^2 + \tau_2^2}{2} = 5.0005 \times 10^{-9} \text{ s}$$
 (2.202)

1642 
$$\langle \tau_D \rangle = \frac{\tau_1 + \tau_2}{2} = 5.05 \times 10^{-5} \text{ s}$$
 (2.203)

1643 
$$\left\langle \tau_D^{-1} \right\rangle = \frac{\tau_1^{-1} + \tau_2^{-1}}{2} = 5.05 \times 10^{+5} \text{ s}$$
 (2.204)

1644 The high frequency relative permittivity is (assuming k = 1 for convenience so that  $C_0 = e_0$ 1645 numerically)

1646 
$$\varepsilon_{\infty} = \frac{C_1 C_2}{e_0 \left(C_1 + C_2\right)} = 5.647$$
 (2.205)

and the low frequency relative permittivity is

1648 
$$\varepsilon_0 = \varepsilon_\infty \frac{\langle \tau_D^2 \rangle}{\langle \tau_D \rangle^2} = (5.647) \frac{(5.005 \times 10^{-9})}{(5.05 \times 10^{-5})^2} = 11.083.$$
 (2.206)

1649 The limiting low and high frequency conductivities are

1650 
$$\sigma_0 = \frac{\epsilon_0 \varepsilon_\infty}{\langle \tau_D \rangle} = \frac{\left(8.854 \times 10^{-12}\right) \left(5.647\right)}{\left(5.05 \times 10^{-5}\right)} = 9.9 \times 10^{-7} \,\mathrm{S \ m^{-1}}$$
 (2.207)

1651 
$$\sigma_{\infty} = \epsilon_0 \varepsilon_{\infty} \langle 1/\tau_D \rangle = (8.854 \times 10^{-12}) (5.647) (5.05 \times 10^{+5}) = 2.53 \times 10^{-5} \text{ Sm}^{-1}.$$
 (2.208)

1652

1653 (1) There are two peaks each in  $\rho''$  and M'' spectra that reflect the different weighting of the 1654 two functions – eqs. (2.184) and (2.186). The two  $\rho''$  peak heights differ by the ratio of the 1655 resistances  $10^8 / 10^6 = 10^2$ , whereas the M'' peaks are equal in height because the two 1656 capacitances are equal. If the capacitances were different and the resistances the same then the 1657 peaks in  $\rho''$  would have the same height and those in M'' would differ. Also  $\rho''$  increases 1658 indefinitely at low frequencies due to  $C_s$  whereas M'' is unaffected.

1659 (2) After subtraction of the contribution of  $\sigma_0$  to  $\varepsilon$ ", and of the limiting high frequency

1660 contribution of  $\varepsilon_{\infty}$  to  $\sigma$ ", both  $\sigma$ " and  $\varepsilon$ " exhibit a single peak at a frequency between the two 1661 maxima exhibited in the *M*" and  $\rho$ " spectra. These single peaks in the admittance functions 1662 occur because at intermediate frequencies the high frequency *RC* element behaves as a 1663 resistance and the low frequency *RC* element behaves as a capacitance. As noted in §2.2.4 the 1664 effectively series *RC* circuit will produce a single loss peak in the admittance, and this is a 1665 disadvantage of admittance functions in analyzing series processes. For the electrode polarization 1666 relaxation caused by *C<sub>s</sub>* in series with the sample resistance  $(R_1 + R_2)$  peaks in  $\sigma$ "- $e_0\varepsilon_{\infty}\omega$  and

- 1667  $\varepsilon'' \sigma_0 / e_0 \omega$  are observed at lower frequencies.
- 1668 (3) A low frequency decrease in  $\sigma'$  and increases in  $\varepsilon'$  and  $\rho''$  are found that due to the 1669 electrode polarization simulated by  $C_s$ . For expositional clarity the value of  $C_s$  was chosen to 1670 ensure a clean separation between the simulated polarization and bulk relaxations but this does 1671 not occur in typical experimental data.
- 1672 The complex plane plots have both advantages and disadvantages compared with the (4)1673 spectra. Two disadvantages are the inconvenience of locating the frequencies of maximum loss, and of comparing these frequencies in  $M^*$  and  $\rho^*$  plots because of the opposite directions of 1674 increasing frequency. On the other hand, complex plane plots are useful for extrapolations. For 1675 example in highly conducting materials whose conductivity relaxation frequency  $1/\langle \tau_{D} \rangle$  lies 1676 above the measuring frequency, and for which electrode polarization is significant or even 1677 severe, the polarization spike in the  $\rho^*$  plane can be extrapolated to the real axis to give an 1678 estimate of  $\sigma_0 = 1/\rho_0$ . At frequencies above the conductivity relaxation frequency,  $\sigma_0$  is 1679 manifested as a spike in the  $\varepsilon^*$  plane, corresponding to the limiting values of 1680  $\lim_{\omega \to 0} \varepsilon'' = \lim_{\omega \to 0} \sigma_0 / \epsilon_0 \omega = \infty \text{ and } \lim_{\omega \to 0} \varepsilon' = \varepsilon_0.$ 1681
- 1682 \*\*\*\*\*\*
- 1683

#### 1684 2.4.6.2 Conductivity Relaxation in Sodium $\beta$ – Alumina

The following permittivity, modulus and resistivity spectra of single crystal sodium  $\beta$ 1685 -alumina at 113 K have been reported by Grant and Ingram [64,65]: (i) the  $\varepsilon$ " spectrum 1686 perpendicular to the conduction planes; (ii) the M'' spectra in orientations perpendicular and 1687 parallel to the conducting planes; (iii) the Z" spectrum in the parallel orientation. The frequency 1688 of maximum Z" in the parallel orientation was close to the frequency of maxima in M" and  $\varepsilon$ " 1689 1690 measured in the perpendicular orientation, and the activation energy for the parallel resistivity 1691 spectrum was close to that for the perpendicular dielectric loss spectrum. The data for the 1692 perpendicular orientation were interpreted in terms of a Maxwell layered dielectric [65], with 1693 each insulating spinel block being a capacitance and each conduction plane a resistance. The activation energy for the dielectric loss was thus determined by that of the conductivity of the 1694 1695 conducting layers, that the data suggest is similar in directions parallel and perpendicular to the conduction planes. The extraordinarily large width of the M<sup>"</sup> spectrum for single crystal Na  $\beta$  – 1696 alumina in the parallel orientation [66,67] indicates a very broad distribution of conductivity 1697 1698 relaxation times, and the resistivity and modulus spectra taken together suggested that the 1699 distribution is bimodal. Grant and Ingram proposed that at 113 K the low frequency conductivity 1700 is determined by an activated localized ion motion that is the same in both orientations. The

# Page 52 of 61

1701 higher frequency conductivity, which contributes to M" but not to  $\rho$ ", results from a relatively 1702 free motion of ions crossing low energy barriers. These mechanisms are consistent with low 1703 temperature localization of sodium ions deduced from NMR data [68]. Localized activation is 1704 not the rate determining step at high temperatures and the well-established low activation energy 1705 for conductivity in sodium  $\beta$ -alumina was observed. The spectra of M<sup>"</sup> and Z<sup>"</sup> for a 1706 representative polycrystalline specimen at 113 K were also shown. The Z" spectrum is 1707 uninformative at this temperature, increasing steadily at low frequencies due to electrode 1708 polarization. The M" spectrum exhibited a maximum at about the same frequency as the single 1709 crystal M'' spectrum observed perpendicular to the conduction planes, and a reproducible 1710 shoulder was observed at about the same frequency as M'' observed parallel to the conduction 1711 planes in single crystals.

1712 This work demonstrates that comparison of the functions M",  $\rho$ " and  $\varepsilon$ " can uncover 1713 details of the conductivity behavior of sodium  $\beta$ -alumina that could not even be discussed if 1714 only  $\sigma^*$  and  $\varepsilon^*$  data were used.

1715

1716 2.4.6.3 Complex Impedance Plane Analysis of Electrode Polarization in Sintered  $\beta$  – 1717 Alumina.

1718 The use of the complex impedance plane for extrapolating polarization phenomena to 1719 obtain data on the bulk material was used extensively by Armstrong and coworkers in their 1720 studies of superionic conductors such as Na  $\beta$ -alumina [55] and Ag-Rb iodide [54-58]. A spike 1721 in the complex impedance plane corresponds to the low frequency increase in Z" due to the 1722 series electrode capacitance and extrapolation of this spike to the real axis yielded the limiting low frequency value of Z' and therefore of  $\rho_0$ . Different surface preparations were observed to 1723 affect the overall impedance but all of the extrapolations gave the same values for  $\rho_0$ . This 1724 method is clearly most appropriate for very highly conducting materials whose conductivity 1725 relaxation lies at frequencies well above those that are experimentally convenient. 1726

1727

1728 2.4.6.4 Complex Impedance Plane Analysis of Atmosphere Dependent Electrode Effects in1729 KHF<sub>2</sub>

1730 Complex impedance plane analysis was also used by Bruinink and Broers [69] for the  $\alpha$ 1731 and  $\beta$  phases of KHF<sub>2</sub>. In an atmosphere of hydrogen with platinum paint electrodes, the 1732 complex impedance plane plot of data for  $\alpha$  -KHF<sub>2</sub> was consistent with a Warburg impedance in 1733 parallel with the bulk resistance and capacitance [69], and extrapolation to the real axis gave a value of  $\rho_0$  in agreement with the separately determined four terminal dc value. This plot gave 1734 no indication of interfacial polarization, consistent with  $\alpha$  -KHF<sub>2</sub> being a proton conductor and 1735 1736 the platinum paint electrodes behaving as reversible hydrogen electrodes. This contrasted sharply with the low frequency behavior of  $\alpha$  -KHF<sub>2</sub> in a vacuum, where a double layer capacitance of 1737 about 440 mF m<sup>-2</sup> per electrode in parallel with a Faradaic resistance of about  $2 \times 10^4 \Omega m$  per 1738 1739 electrode produced an additional semicircle in the complex plane. For the polycrystalline  $\beta$ 1740 -phase the complex plane plot was essentially unchanged for data taken in both a hydrogen 1741 atmosphere and a vacuum [69] and is consistent with a Warburg impedance in series with a 1742 parallel RC element, corresponding to electrode polarization due to blocking of  $K^+$  and/or  $F^-$ 

charge carriers. An *RC* transmission line was used to rationalize the Warburg impedance in terms of bulk electrical relaxation.

1745

# 1746 2.4.6.5 Intergranular Effects in Polycrystalline Electrolytes

1747 The effects of intergranular material on the overall electrical response of polycrystalline electrolytes have been extensively documented. Only one example is discussed here [9,66]. The 1748 1749 simplest equivalent circuit representation of such materials comprises two parallel RC elements 1750 in series, where one element is associated with a crystallite and the other with intergranular 1751 material. Armstrong et al. [70] have shown that such a series circuit can represent the principle 1752 features of polycrystalline electrolytes. Since the interface is thin and the permittivities of ionic 1753 solids typically vary by a factor of less than 10, the capacitance  $C_i$  associated with the interface is 1754 much higher than that of the grain  $C_p$ :

1755 
$$C_i = \frac{\epsilon_0 \varepsilon' A_i}{d_i} >> \epsilon_0 \varepsilon' = k C_p$$
(2.209)

where  $A_i$  is the average cross section area,  $d_i$  is the average thickness of the intergranular material, and  $k = e_0 / C_0$  is the cell constant.

1758

1759 2.4.6.6 Intergranular Cracking

Experimental M" and  $\rho$ " spectra for a polycrystalline material known to have 1760 1761 intergranular cracking were shown in reference [9]. The spectra were similar to those for two parallel  $R_p C_p$  elements in series although the experimental peaks were broader - they could be 1762 approximated as the sum of two Debye peaks of equal heights separated by about a decade in 1763 frequency, so that the maxima in Z" and M" could be approximated as  $R_p/4$  and  $C_0/4C_p$ , 1764 respectively. Computed values of R and C for the intergranular and granular material in the 1765 1766 cracked sample, using these approximations and assuming a resolution into symmetric  $\rho$ " peaks, are: 1767

1768 Lower Frequency (Intergranular) Relaxation in Cracked Sample

1769 
$$\tau_i = \frac{1}{\omega_{\max(Z'')}} = 6.4 \times 10^{-6} \text{ s},$$
 (2.210)

1770 
$$R_i \approx 4Z_{\text{max}} = 6.4 \times 10^6 \,\Omega,$$
 (2.211)

1771 
$$C_i = \frac{\tau_i}{R} \approx 1.0 \,\mathrm{pF}.$$
 (2.212)

1772 Higher frequency (Intragranular) Relaxation in Cracked Sample

1773 
$$au_c = \frac{1}{\omega_{\max(Z'')}} = 1.6 \times 10^{-7} \text{ s},$$
 (2.213)

1774 
$$R_c \approx 4Z_{\text{max}} = 2.6 \times 10^6 \,\Omega,$$
 (2.214)

1775 
$$C_c = \frac{\tau_c}{R_c} \approx 0.06 \,\mathrm{pF}$$
 (2.215)

1776 The impedance spectrum was drastically altered after annealing out of the intergranular

#### Page 54 of 61

1777 cracking [9] (Figure 2.14(C)). The remaining single peak in Z" was essentially indistinguishable 1778 from the high frequency peak in the cracked material, strongly suggesting that it was due to 1779 intra-crystal relaxation and that the additional low frequency peak for the unannealed sample is 1780 due to cracking and the consequent air gaps. Consistent with this, the modulus spectrum was 1781 essentially unchanged by annealing since it is unaffected by the high capacitance cracks. These estimates of the intragranular and intergranular resistances were confirmed by the  $\sigma_0$  data: the 1782 observed conductivity of the cracked sample was largely determined by the intergranular 1783 1784 resistance, and the ratio of the conductivities of the sample before and after annealing should 1785 have been

1786 
$$\frac{Z_{\max}^{nlow\omega} + Z_{\max}^{nligh\omega}}{Z_{\max}^{nligh\omega}} = \frac{2.25 \times 10^6}{0.65 \times 10^6} = 3.5, \qquad (2.216)$$

1787 in fair agreement with

1791

1788 
$$\frac{\sigma_{annealed}}{\sigma_{cracked}} = 3.1. \tag{2.217}$$

1789 The combination of modulus and impedance spectroscopies once again revealed details that 1790 could not be obtained from the original  $\sigma'$  and  $\varepsilon'$  data.

1792 2.4.6.7 Intergranular Gas Adsorption

1793 The effects of oxygen and alkali doping on the electrical response of polycrystalline zinc 1794 oxide were studied by Seitz and Sokoly [71]. Only the effects of oxygen pressure are discussed 1795 here. An increase in conductivity was observed with decreasing oxygen pressure and the absence 1796 of changes due to different electrode materials implied that adsorbed oxygen at grain surfaces 1797 was responsible for the observed polarization of the sample. The conductivity and permittivity 1798 were plotted explicitly as a function of frequency in this report and these data allowed M'' and 1799  $\rho$ " spectra to be calculated without difficulty. The calculated M" and  $\rho$ " spectra exhibited two partially resolved peaks whose estimated magnitudes are consistent with a thin (high 1800 capacitance) high resistance layer determining the low frequency response. Both peaks in the M''1801 spectrum have comparable half widths (ca. 1.5 decades) and their relative maximum values 1802  $(8 \times 10^{-4})$  and  $(1.1 \times 10^{-2})$  are a good (inverse) measure of the relative capacitance of each 1803 relaxation:  $C_{\ell} / C_{h} \approx 13$ . The resistance ratio  $R_{\ell} / R_{h}$  of the low frequency high frequency 1804 relaxation can then be estimated from the two values of  $f_{\rm max}$  (ca. 5×10<sup>2</sup> and 3×10<sup>5</sup> Hz) to be 1805 1806 about 45:

1807 
$$\frac{R_{\ell}C_{\ell}}{R_{h}C_{h}} \approx 600 \approx \frac{13R_{\ell}}{R_{h}} \Longrightarrow \frac{R_{\ell}}{R_{h}} \approx 45.$$
(2.218)

1808 The conductivity estimated from the height of the lower frequency resistivity peak is  $1.1 \times 10^{-7}$ 1809 S/m, in reasonable agreement with the low frequency plateau value of  $1.3 \times 10^{-7}$  S/m. From the 1810 relative frequencies of the *M*" maxima and the relative heights of the (partly resolved)  $\rho$ " 1811 maxima, the conductivity of the high frequency relaxation is estimated to be about  $10^{-6\pm 1}$ . 1812 Because of its higher associated capacitance the lower frequency relaxation almost certainly 1813 corresponds to an intergranular impedance, and its removal by a reduction in oxygen pressure 1814 should therefore increase the sample conductivity by about 45 but have a small effect on the measured permittivity (since removal of a high series capacitance has little effect). This predicted
change in resistivity agrees with the qualitative statement that conductivity increased with
decreasing oxygen pressure [71].

Page 56 of 61

- 1819 Appendices
- 1821 Appendix 2.1 – Derivation of  $M^*$  for a Debye Relaxation with No Additional Separate 1822 Conductivity
  - These derivations are shown for pedagogical clarity rather than mathematical elegance.

1824 (1) 
$$\Delta \varepsilon \equiv \varepsilon_0^E - \varepsilon_\infty^E; \tau_D = \left(\varepsilon_\infty^E / \varepsilon_0^E\right) \tau_E; M_0^E = 1 / \varepsilon_0^E; M_\infty^E = 1 / \varepsilon_\infty^E$$

1825 (2) 
$$M^* = 1/\varepsilon^* \Longrightarrow M' = \frac{\varepsilon'}{\varepsilon'^2 + \varepsilon''^2}; M'' = \frac{-\varepsilon''}{\varepsilon'^2 + \varepsilon''^2}$$

1826 (3) 
$$\varepsilon' = \varepsilon_{\infty}^{E} + \frac{\left(\varepsilon_{0}^{E} - \varepsilon_{\infty}^{E}\right)}{1 + \omega^{2}\tau_{E}^{2}} = \varepsilon_{\infty}^{E} + \frac{\Delta\varepsilon}{1 + \omega^{2}\tau_{E}^{2}}; \varepsilon'' = \frac{\Delta\varepsilon\omega\tau_{E}}{1 + \omega^{2}\tau_{E}^{2}}$$
$$\varepsilon''^{2} + \varepsilon''^{2} = \left(\varepsilon_{\infty}^{E}\right)^{2} + \frac{2\varepsilon_{\infty}^{E}\Delta\varepsilon}{1 + \omega^{2}\tau_{E}^{2}} + \frac{\Delta\varepsilon^{2}}{\left(1 + \omega^{2}\tau_{E}^{2}\right)^{2}} + \frac{\Delta\varepsilon^{2}\omega^{2}\tau_{E}^{2}}{\left(1 + \omega^{2}\tau_{E}^{2}\right)^{2}}$$

1827

1820

1823

$$=\frac{\left(\varepsilon_{\infty}^{E}\right)^{2}\left(1+\omega^{2}\tau_{E}^{2}\right)+2\varepsilon_{\infty}^{E}\Delta\varepsilon+\Delta\varepsilon^{2}}{1+\omega^{2}\tau_{E}^{2}}=\frac{\left(\varepsilon_{0}^{E}\right)^{2}+\left(\varepsilon_{\infty}^{E}\right)^{2}\omega^{2}\tau_{E}^{2}}{1+\omega^{2}\tau_{E}^{2}}$$

$$M' = \left(\frac{\varepsilon_{\infty}^{E} \left(1 + \omega^{2} \tau_{E}^{2}\right) + \Delta \varepsilon}{1 + \omega^{2} \tau_{E}^{2}}\right) \left(\frac{1 + \omega^{2} \tau_{E}^{2}}{\left(\varepsilon_{0}^{E}\right)^{2} + \left(\varepsilon_{\infty}^{E}\right)^{2} \omega^{2} \tau_{E}^{2}}\right) = \left(\frac{\varepsilon_{0}^{E} + \varepsilon_{\infty}^{E} \omega^{2} \tau_{E}^{2}}{\left(\varepsilon_{0}^{E}\right)^{2} + \left(\varepsilon_{\infty}^{E}\right)^{2} \omega^{2} \tau_{E}^{2}}\right) = \left[\frac{\varepsilon_{0}^{E} + \varepsilon_{\infty}^{E} \omega^{2} \tau_{E}^{2}}{\left(\varepsilon_{0}^{E}\right)^{2} + \left(\varepsilon_{\infty}^{E}\right)^{2} \omega^{2} \tau_{E}^{2}}\right] = \left[\frac{\varepsilon_{0}^{E} + \varepsilon_{\infty}^{E} \omega^{2} \tau_{E}^{2}}{\left(\varepsilon_{0}^{E}\right)^{2} + \left(\varepsilon_{\infty}^{E}\right)^{2} \omega^{2} \tau_{E}^{2}}\right]$$

1828

$$(4) \qquad = \frac{1}{\varepsilon_{0}^{E}} + \frac{\varepsilon_{\infty}^{E}\omega^{2}\tau_{E}^{2} - \frac{\varepsilon_{\infty}^{2}}{\varepsilon_{0}}\omega^{2}\tau_{E}^{2}}{\left(\varepsilon_{0}^{E}\right)^{2}\left(1 + \frac{\left(\varepsilon_{\infty}^{E}\right)^{2}}{\left(\varepsilon_{0}^{E}\right)^{2}}\omega^{2}\tau_{E}^{2}\right)} = \frac{1}{\varepsilon_{0}^{E}} + \frac{\frac{\varepsilon_{\infty}^{E}}{\left(\varepsilon_{0}^{E}\right)^{2}}\omega^{2}\tau_{E}^{2}}{\left(1 + \frac{\left(\varepsilon_{\infty}^{E}\right)^{2}}{\left(\varepsilon_{0}^{E}\right)^{2}}\omega^{2}\tau_{E}^{2}\right)} = \frac{1}{\varepsilon_{0}^{E}} + \frac{\frac{\varepsilon_{\infty}^{E}}{\left(\varepsilon_{0}^{E}\right)^{2}}\omega^{2}\tau_{E}^{2}}{\left(1 + \frac{\left(\varepsilon_{\infty}^{E}\right)^{2}}{\left(\varepsilon_{0}^{E}\right)^{2}}\omega^{2}\tau_{E}^{2}\right)} = \frac{1}{\varepsilon_{0}^{E}} + \frac{\frac{\varepsilon_{\infty}^{E}}{\left(\varepsilon_{0}^{E}\right)^{2}}\omega^{2}\tau_{E}^{2}}{\left(1 + \frac{\varepsilon_{\infty}^{E}}{\left(\varepsilon_{0}^{E}\right)^{2}}\omega^{2}\tau_{E}^{2}\right)} = \frac{1}{\varepsilon_{0}^{E}} + \frac{\varepsilon_{\infty}^{E}}{\left(1 + \frac{\varepsilon_{\infty}^{E}}{\left(\varepsilon_{0}^{E}\right)^{2}}\omega^{2}\tau_{E}^{2}\right)} = \frac{1}{\varepsilon_{0}^{E}} + \frac{\varepsilon_{\infty}^{E}}{\left(1 + \frac{\varepsilon_{\infty}^{E}}{\left(\varepsilon_{0}^{E}\right)^{2}}\omega^{2}\tau_{E}^{2}\right)}{\left(1 + \frac{\varepsilon_{\infty}^{E}}{\left(1 + \frac{\varepsilon_{\infty}^{E}}{\left(\varepsilon_{0}^{E}\right)^{2}}\right)} = M_{0}^{E} + \frac{\varepsilon_{0}^{E}}{\left(1 + \frac{\varepsilon_{0}^{E}}{\left(1 + \omega^{2}\tau_{D}^{2}\right)}\right)}{\left(1 + \omega^{2}\tau_{D}^{2}\right)}$$

$$M'' = \left(\frac{-\Delta\varepsilon\omega\tau_{E}^{2}}{1+\omega^{2}\tau_{E}^{2}}\right) \left(\frac{1+\omega\tau_{E}^{2}}{\left(\varepsilon_{0}^{E}\right)^{2}+\left(\varepsilon_{\infty}^{E}\right)^{2}\omega^{2}\tau_{E}^{2}}\right) = \left(\frac{-\Delta\varepsilon\omega\tau_{E}}{\left(\varepsilon_{0}^{E}\right)^{2}\left(1+\frac{\left(\varepsilon_{\infty}^{E}\right)^{2}}{\left(\varepsilon_{0}^{E}\right)^{2}}\omega^{2}\tau_{E}^{2}\right)}\right)$$
(5)

1830

$$= \left(\frac{-\Delta\varepsilon \frac{1}{\varepsilon_0 \varepsilon_\infty^E} \frac{\varepsilon_\infty^E}{\varepsilon_0^E} \omega \tau_E}{\left(1 + \frac{\left(\varepsilon_\infty^E\right)^2}{\left(\varepsilon_0^E\right)^2} \omega^2 \tau_E^2\right)}\right) = \frac{\left(M_\infty^E - M_0^E\right) \omega \tau_D}{\left(1 + \omega^2 \tau_D^2\right)}$$

1831

1832A Matlab®/Octave program for computing the components of  $M^*$  with added conductivity is1833given below in Appendix 2.2.

Page 58 of 61

- 1835 Appendix 2.2 Matlab®/GNU Octave Codes
- 1836 Computation Code for a Debye Relaxation with Additional Separate Conductivity  $\sigma_0$ .
- 1837 The algebraic derivation is excessively tedious and is replaced here by a 1838 Matlab®/GNUOctave code that plots both components of the  $\varepsilon^*$  and  $M^*$  functions. The values 1839 of the input parameters are entered by editing the m-file.
- 1840
- 1841 % FUNCTION DebyeCondM Computes and Plots M\* for Debye E\* plus constant conductivity
- 1842 function HD = DebyeCondM
- 1843 w = logspace(-6, +6, 1200);
- 1844 Logw = log10(w);
- 1845 E00 = 8.854E-12; % Vacuum permittivity in F/m
- 1846 E0D = 20; % Low f dielectric relative permittivity
- 1847 EinfD = 10; % High f dielectric relative permittivity
- 1848 DelE = E0D EinfD; % Dielectric dispersion range
- 1849 EinfE = 3; % High f conductivity relative permittivity
- 1850 TauD =  $10^{-4}$  % Dielectric relaxation time
- 1851 Sigma $0 = 10^{-15}$ ; % Conductivity in S/m
- 1852 Tausig = E00\*EinfE/Sigma0 % Conductivity relaxation time
- 1853 E2sig = Sigma0./(E00\*w); % Conductivity contribution to E2
- 1854 % CALCULATE E1 and E2
- 1855 wTauD = w\*TauD;
- 1856 Num =  $1./(1 + wTauD.^2);$
- 1857 E1 = EinfD + DelE\*Num; %Debye E1
- 1858 E2 = DelE\*wTauD.\*Num + E2sig; % Debye E2 + Conductivity E2
- 1859 Denom =  $E1.^{2} + E2.^{2}$ ;
- 1860 M1 = E1./Denom;
- 1861 M2 = E2./Denom;
- 1862 subplot (2,2,1);
- 1863 plot (Logw, E1);
- 1864 ylabel("E1");
- 1865 subplot (2,2,2);
- 1866 plot (Logw, E2);
- 1867 ylabel("E2");
- 1867 yiabel(122), 1868 subplot (2,2,3);
- 1868 subplot (2,2,3); 1869 plot (Logw, M1);
- 1800 plot (Logw, M1) 1870 ylabel("M1");
- 1871 subplot (2,2,4);
- 1872 plot (Logw, M2);
- 1873 ylabel("M2");
- 1874
- 1875 return
- 1876

(C4)

- 1877 Appendix 2.3 Derivation of Debye Dielectric Expression from Equivalent Circuit
- 1878 Impedance of  $R_s + C_s$  is  $Z_{s} = R_{s} + 1/i\omega C_{s} = (1 + i\omega R_{s}C_{s})/i\omega C_{s} = (1 + i\omega \tau_{s})/i\omega C_{s}$ 1879 (C1) 1880 and its admittance is

1881 
$$A_s = 1/Z_s = i\omega C_s / (1 + i\omega \tau_s)$$
(C2)

where  $\tau_s \equiv R_s C_s$ . The total admittance is 1882

1883 
$$A^* = i\omega C_s / (1 + i\omega \tau_s) + G_p + 1 / (i\omega C_p)$$
(C3)

1884 and the complex capacitance is  

$$C^* = A^*/i\omega = C_p + C_s / (1 + i\omega\tau_s) + G_p / i\omega$$

$$= \frac{C_p (1 + i\omega\tau_s) + C_s}{1 + i\omega\tau_s} + \frac{G_p}{i\omega} = \frac{\left[C_p (1 + i\omega\tau_s) + C_s\right](1 - i\omega\tau_s)}{1 + \omega^2\tau_s^2} + \frac{G_p}{i\omega}$$
1885
$$= \frac{\left[C_p (1 + \omega^2\tau_s^2) + C_s (1 - i\omega\tau_s)\right]}{1 + \omega^2\tau_s^2} - \frac{iG_p}{\omega}$$

$$= \frac{\left[C_p (1 + \omega^2\tau_s^2) + C_s\right]}{1 + \omega^2\tau_s^2} - \frac{i\omega\tau_s C_s}{1 + \omega^2\tau_s^2} - \frac{iG_p}{\omega}$$
1895

1886 from which eqs. (2.153) and (2.154) obtain.

1887

Page 60 of 61

- 1888 REFERENCES (Needs Updating)
- 1889 [1] I. M. Hodge, K. L. Ngai, C. T. Moynihan, J. Non-Cryst. Solids <u>351</u> 104 (2005)
- 1890 [2] G. W. Chantry, "Long-wave Optics", Academic (1984), ISBN 0-12-168101-7
- 1891 [3] N. F. Hill, W. E. Vaughan, A. H. Price, and M. Davies, "Dielectric Properties and Molecular Behavior", p. 112, Van Nostrand (1969)
- 1893 [4] L. Onsager, J. Am. Chem. Soc. <u>58</u> 1486 (1936)
- 1894 [5] J. G. Kirkwood, J. Chem. Phys. <u>7</u> 911 (1939)
- 1895 [6] H. Frohlich, "*Theory of Dielectrics*", 2<sup>nd</sup> Ed. Vol <u>2</u> 72-73 (1958)
- 1896 [7] R. D. Mountain, *Proc. NYAS* <u>371</u> 252 (1981)
- 1897 [8] E. Fatuzzo and P. R. Mason, *Proc. Phys. Soc.* <u>90</u> 741 (1967)
- 1898 [9] R. L. Fulton, Mol. Phys. <u>29</u> 405 (1975)
- 1899 [10] I. M. Hodge, M. D. Ingram and A. R. West, J. Electroanal. Chem. <u>74</u> 125 (1976)
- 1900 [11] R. D. Armstrong, W. P. Race and H. R. Thirsk, *Electrochim Acta*. <u>13</u> 215 (1968)
- 1901 [12] R. D. Armstrong and R. Mason, J. Electroanal. Chem. <u>41</u>, 231 (1973)
- 1902 [13] R. D. Armstrong, J. Electroanal. Chem. <u>52</u> 413 (1974)
- 1903 [14] E. Warburg, *Wied. Ann.* <u>67</u> 493 (1899)
- 1904 [15] E. Warburg, Ann. Phys. <u>6</u> 125 (1901)
- 1905 [16] R. D. Armstrong, J. Electroanal. Chem. <u>52</u> 413 (1974)
- 1906 [17] D. Miliotis and D. N. Voon, J. Phys. Chem. Solids <u>30</u> 1241 (1969)
- 1907 [18] J. M. Wimmer and N. M. Tallan, J. Appl. Phys. <u>37</u> 3728 (1966)
- 1908 [19] R. D. Armstrong and R. A. Burnham, J. Electroanal. Chem. <u>72</u> 257 (1976)
- 1909 [20] R. D. Armstrong and K. Taylor, *J. Electroanal. Chem.* <u>63</u> 9 (1975)
- 1910 [21] R. Richert, Adv. Chem. Phys. <u>156</u> 101 (2014)
- 1911 [22] E. Bauer, *Cah. Phys.* <u>20</u> 1 (1944)
- 1912 [23] J. M. Stevels, *Handbuch der Physik*, Vol XX 372 (1957)
- 1913 [24] S. Glasstone, K. J. Layler and H. Eyring, "*The Theory of Rate Processes*", McGraw-Hill, 1914 New York, (1941)
- 1915 [25] H. E. Taylor, J. Soc. Glass Technol. <u>43</u> 124 (1959)
- 1916 [26] R. J. Charles, J. Appl. Phys. <u>32</u> 1115 (1961)
- 1917 [27] J. O. Isard, Proc. Inst. Elect. Engrs., Supplement No. 20 <u>109B</u>, 440 (1962)
- 1918 [28] J. O. Isard, J. Non. Cryst. Solids <u>4</u> 357 (1970)
- 1919
   [29]
   G. Williams, D. C. Watt, S. B. Dev and A. M. North, *Trans. Faraday Soc.* <u>67</u> 1323

   1920
   (1971)
- 1921 [30] G. Williams and D. C. Watt, *Trans. Faraday Soc.* <u>66</u> 80 (1970)
- 1922 [31] P. Debye, "Polar Molecules", Chapter 1, Chemical Catalog Co., New York, (1929)
- 1923 [32] L. Hayler and M. Goldstein, J. Chem. Phys. <u>66</u> 4736 (1977)
- 1924 [33] N. G. Crum, B. E. Read, and G. Williams, "Anelastic and Dielectric Effects in Polymeric 1925 Solids", Dover, New York (1991)
- 1926 [34] K. W. Wagner, Arch. Electrotech. <u>2</u> 378 (1914)
- 1927 [35] R. W. Sillars, J. Inst. Electr. Engrs <u>80</u> 378 (1937)
- 1928 [36] L. K. H. van Beek, *Physica* <u>26</u> 66 (1960)
- 1929 [37] I. M. Hodge and C. A. Angell, *J. Chem. Phys.* <u>68</u> 1363 (1978)
- 1930 [38] J. B. Hasted and M. Shahadi, *Nature* <u>262</u> 777 (1976)
- 1931 [39] I. M. Hodge and C. A. Angell, J. Phys. Chem. <u>82</u> 1761 (1978)
- 1932 [40] G. S. Darbari and S. Petrucci, *J. Phys. Chem.* <u>73</u> 921 (1969)

- 1933 [41] G. S. Darbari, M. R. Richelson and S. Petrucci, J. Chem. Phys. 53 859 (1970) 1934 J. E. Enderby and G. W. Neilsen, in "Water. A Comprehensive Treatise", Vol 6", Ed. F. [42] 1935 Franks Plenum, New York (1978) 1936 D. Bertolini, M. Cassetteri and G. Salvetti, J. Phys. Chem 76 3285 (1982) [43] 1937 P. B. Macedo, C. T. Moynihan and R. Bose, Phys. Chem. Glasses 13 171 (1972) [44] C. Kittel, "Introduction to Solid State Physics", 7th Ed., Wiley, (1996) 1938 [45] 1939 [46] G. P. Johari and K. Pathmanathan, Phys. Chem. Glasses 29 219 (1988) 1940 [47] I. M. Hodge and C. A. Angell, J. Chem. Phys. 67 1647 (1977) 1941 [48] F. S. Howell, *Ph.D. Thesis*, Catholic University of America (1972) 1942 [49] I. M. Hodge and C. A. Angell, J. Phys. Chem. 82 1761 (1978) 1943 H. P. Schwan, G. Schwarz, J. Maczak and H. Pauly, J. Phys. Chem. 66, 2626 (1962) [50] 1944 [51] D. P. Almond & A. R. West, J. Non-Cryst. Solids 88 222 (1986) 1945 [52] D. Ravaine and J.-L. Souquet, J. Chim. Phys. 71 693 (1974) 1946 D. Ravaine, J. P. Diard and J. -L. Souquet, Faraday Trans. II, 1935 (1975) [53] K. S. Cole and R. H. Cole, J. Chem. Phys. 9 341 (1949) 1947 [54]. 1948 [55] R. D. Armstrong and R. A. Burnham, J. Electroanal. Chem. 72 257 (1976) 1949 R. D. Armstrong and W. I. Archer, *ibid*, 87 221 (1978) [56] 1950 [57] R. D. Armstrong, T. Dickinson and P. M. Willis, J. Electroanal. Chem. 48 47 (1973) 1951 [58] R. D. Armstrong, T. Dickinson and P. M. Willis, J. Electroanal. Chem. 54 281 (1975) 1952 R. D. Armstrong and K. Taylor, J. Electroanal. Chem. 63 9 (1975) [59] 1953 [60] J. E. Bauerle, J. Phys. Chem. Solids <u>30</u> 2657 (1969) 1954 R. J. Grant, M. D. Ingram and A. R. West, *Electrochim. Acta* 22 729 (1977) [61] 1955 M. Pollak and T. H. Geballe, *Phys. Rev.* <u>122</u> 1742 (1961) [62] 1956 D. W. Davidson and R. H. Cole, J. Chem. Phys. 18 1417 (1951) [63] 1957 [64] R. J. Grant and M. D. Ingram, J. Electroanal. Chem. 83 199 (1977) R. J. Grant, M. D. Ingram and A. R. West, J. Electroanal. Chem 74 125 (1976) 1958 [65] 1959 [66] I. M. Hodge, R. J. Grant, M. D. Ingram and A. R. West, Nature 266 42 (1977) 1960 R. J. Grant, M. D. Ingram and A. R. West, *Electrochim. Acta* 22 729 (1977) [67] 1961 [68] E. Lang and H. –D. Ludemann, Angew Chem. Int. Eng. 21 315 (1982) 1962 J. Bruinink and G. H. J. Broers, J. Phys. Chem. Solids 33 1713 (1972) [69] 1963 [70] R. D. Armstrong, T. Dickinson and P. M. Willis, Electroanal. Chem & Interfac. 1964 *Electrochem.* 53 389 (1974) 1965 [71] M. A. Seitz and T. L. Sokoly, J. Electrochem. Soc. <u>121</u> 163 (1974) 1966 [72] I. M. Hodge and A. Eisenberg, *Macromolecules* 11 283 (1978)
- 1967